Advanced Materials

ADVANCED MATERIALS
www.advmat.de

PERSPECTIVE OPEN ACCESS
Editor's Choice

Chiral Metal Halide Perovskites for Spin-Polarized Light-Emitting Diodes

Ashish Gaurav[1] | Jihyun Kim[1,4] | Nadesh Fiuza-Maneiro[2] | Hongki Kim[3] | Hae-Jun Seok[1] | Sergio Gómez Grana[2] | Robert L. Z. Hoye[1] | Lakshminarayana Polavarapu[2] | Matthew J. Fuchter[3,4]

[1]Inorganic Chemistry Laboratory, Department of Chemistry, University of Oxford, Oxford, UK | [2]CINBIO, Universidade de Vigo, Materials Chemistry and Physics Group, Department of Physical Chemistry, Campus Universitario Lagoas Marcosende, Vigo, Spain | [3]Department of Chemistry, Molecular Sciences Research Hub, Imperial College London, London, UK | [4]Department of Chemistry, Chemistry Research Laboratory, University of Oxford, Oxford, UK

Correspondence: Robert L. Z. Hoye (robert.hoye@chem.ox.ac.uk) | Lakshminarayana Polavarapu (lakshmi@uvigo.gal) | Matthew J. Fuchter (matthew.fuchter@chem.ox.ac.uk)

Received: 23 December 2025 | **Revised:** 4 March 2026 | **Accepted:** 11 March 2026

Keywords: chiral metal-halide perovskites | circular polarization | perovskite nanocrystals | spin-LEDs

ABSTRACT

With the growing importance of displays, reducing their power consumption has become crucial for developing energy-efficient photonic–electronic platforms. Conventional light emitting diodes (LEDs) rely on external polarizers and waveplates to control light polarization in displays, but these optics cause at least half of the incident energy of the LEDs to be lost, demanding higher drive currents and accelerating degradation. Generating circularly polarized light (CPL) directly at the source offers a low-power alternative by eliminating such optical losses and enabling direct spin–photon interfaces. Recently, chiral metal halide perovskites (MHPs) have emerged as efficient, solution-processable semiconductors that intrinsically couple light polarization and spin. Their strong spin–orbit coupling and broken inversion symmetry enable spin-selective charge transport via the chiral-induced spin selectivity effect, allowing both spin manipulation and its impact on emission to be observed within the same layer. In colloidal nanocrystal form they can emit CPL with high photoluminescence quantum yield, making them promising candidates for chiral light emission, although their use is still limited by low polarization anisotropy. This perspective discusses intrinsic and extrinsic routes to achieve circularly polarized electroluminescence (CP-EL) using chiral MHPs, highlights progress in low-dimensional films and chiral-ligand nanocrystals, and discusses prospects for room-temperature spin control and filter-free, spin-LEDs for next-generation energy-efficient optoelectronic displays.

1 | Introduction

Light-emitting diodes (LEDs) have progressed from simple electroluminescent (EL) indicators to high-performance, color-tunable light sources that are foundational to modern display and lighting technologies [1–3]. However, because their emission is largely unpolarized, ambient reflections can degrade contrast at high luminance. To mitigate this, display stacks commonly integrate an external circular polarizer to impose a defined state and reduce glare [4]. Among various aspects, controlling the emission polarization state at the light source has become essential, not only to enhance display contrast and suppress glare, but also to enable emerging photonic and spintronic functionalities. Polarized light refers to a well-defined orientation of a light wave's transverse electric field, and therefore also its magnetic field, relative to the direction of propagation. In linear

Ashish Gaurav and Jihyun Kim contributed equally to this work.

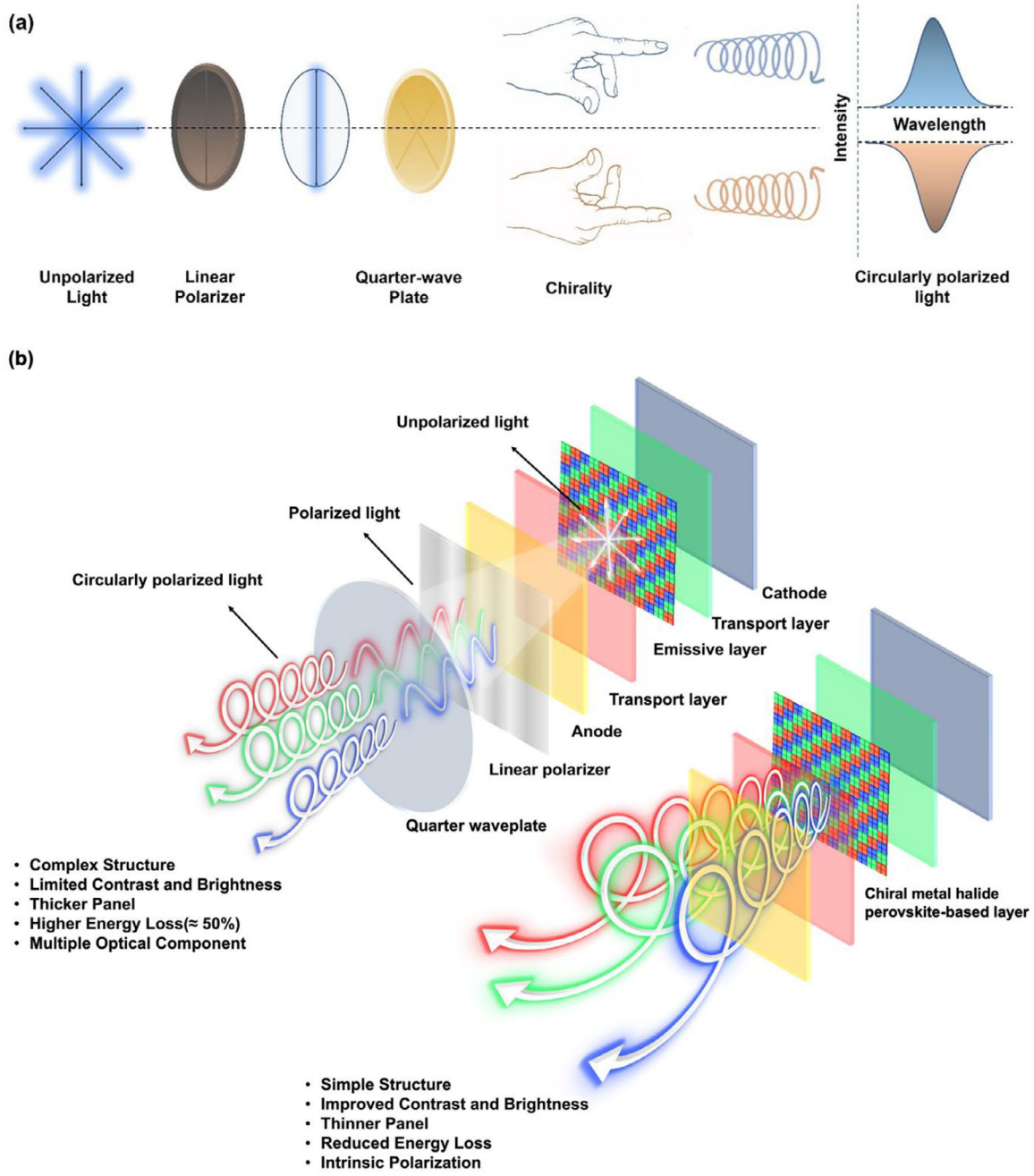

FIGURE 1 | a) Schematic of circular polarization: linearly polarized light modulated by a quarter-wave plate to produce left- and right-handed CPL. b) Comparison of conventional displays (top) and architectures incorporating chiral MHP layers (bottom). Conventional devices rely on external polarizers and waveplates, leading to ~50% energy loss, whereas a chiral MHP layer, used either as the emissive layer or as a spin-filter in front of an achiral emitter, can intrinsically generate or select circularly polarized light, enabling simpler, brighter and more efficient displays.

polarized light the field oscillates in one fixed plane, whereas, in circular polarized light (CPL) two orthogonal components of equal amplitude with a $\pm \pi/2$ phase shift make the field rotate helically in either a left- or right-handed screw sense (Figure 1a). Elliptically polarized light is the general case between these states.

Among polarized light states, CPL is of particular interest because the handedness of its polarization provides an additional degree of freedom beyond brightness and color. Key applications that use or benefit from CPL include 3D displays, optical sensing, and optical data storage, and CPL can be generated directly by devices such as spin-LEDs [5, 6]. To achieve CPL emission from a conventional LED, unpolarized emission is first set to a single linear state by an external linear polarizer and then converted to circular polarization by a quarter-wave plate (QWP) [7]. The implications of CPL generation for display technologies are summarized in Figure 1b, which contrasts conventional polarization optics with architectures incorporating chiral MHP layers that can generate or select CPL within the device stack. Because polarization optics discard a substantial fraction of the emitted photons, maintaining a target luminance typically requires higher drive power, increasing power consumption and heat load and

potentially shortening operational lifetime. These considerations motivate strategies that generate or select well-defined circular polarization within the emissive stack, rather than filtering it after emission.

To reduce the optical losses caused by external polarizers, researchers have developed chiral (spin)-LEDs that emit left- or right-handed CPL directly from the emitting layer [8, 9]. In these devices, the molecular or structural chirality of the emissive material or charge transport layers control CPL through optical transitions or spin-selective recombination, removing the need for external filters. A widely used parameter of chiroptical performance in luminescent and absorbing materials is the dissymmetry factor, g, defined generally by $g = \frac{2(I_L - I_R)}{I_L + I_R}$, where I_L and I_R are the intensities of the left- and right-circularly polarized components of the optical signal. This definition applies equivalently to absorption (g_{abs}), photoluminescence (g_{PL}), and electroluminescence (g_{EL}). This approach has been demonstrated using a wide range of materials, including chiral small molecules and π-conjugated polymers (often with chiral side groups), twisted fibers, chiral metal complexes, chiral semiconductor nanocrystals (NCs), and non-chiral emitters placed in chiral optical structures [10–14]. However, most molecular chiral emitters still face fundamental limitations. Their chiroptical activity is generally weak ($|g_{PL}| \approx 10^{-4}$–10^{-2}, due to the coupling between electric and (weak) magnetic dipole transitions. As a result, achieving both high polarization anisotropy and device efficiency remains challenging [15]. Moreover, precise control over film morphology and long-term stability is often difficult [16, 17].

To overcome these constraints, chiral metal halide perovskites (MHPs) have recently emerged as a promising alternative to existing materials. These materials exhibit high photoluminescence quantum yields (PLQYs), and their combination of strong spin–orbit coupling (SOC) and broken inversion symmetry can produce large chiroptical responses. Furthermore, composition- and dimensional-tunability and low-temperature solution processability are possible. These materials can also function simultaneously as chiral emitters and spin filters, enabling polarized light emission to be directly produced without need for polarizers [18–21]. Spin filtering in chiral MHPs arises from chiral-induced spin selectivity (CISS). There is still significant debate about the precise mechanism(s) of CISS and how such mechanism(s) vary in different material sets. However, it is broadly proposed that a non-magnetic chiral crystal potential, amplified by strong SOC, couples carrier spin to momentum, making transmission (T) inherently spin dependent ($T_{spin-up} \neq T_{spin-down}$) [22]. One spin orientation is therefore preferentially transmitted through a given enantiomer, while the opposite is suppressed. The sign of the polarization is therefore set by the *R/S* enantiomer.

In device-relevant implementations, chiral MHPs are realized by two solution-processed routes: (i) low-dimensional (0D/1D/2D) layered films grown with chiral ammonium cations, where the chiral molecules impart chirality to MHPs and the reduced dimensionality strengthens chiroptical response; and (ii) colloidal NCs rendered chiral via surface binding of chiral ligands that induce lattice distortion. Halide stoichiometry (Cl/Br/I) tunes the bandgap and thus the emission color. Both formats can be integrated into spin-LEDs, with layered chiral MHPs films interfacing with other emissive materials to act as CISS-based spin filters. Through this interfacial coupling, spin-polarized carriers are generated within the active stack, enabling source-level CP-EL at room temperature, further quantified as g_{EL} [23]. On the other hand, chiral NCs can be directly used as an emitter where carriers combine and result in CP-EL.

Accordingly, chiral MHPs have rapidly evolved from structurally interesting curiosities into a versatile family of functional opto-electronic materials. As summarized in Figure 2, the field began with the first report of a chiral MHP single-crystal by Billing et al. in 2003 [24], followed by the synthesis of helical chiral MHPs [25], and later 2D chiral hybrid MHPs films whose chiroptical responses were quantitatively measured [26]. Subsequent studies extended chirality to MHPs NCs [27, 28] and nanoplatelets [29]. These works demonstrated 2D chiral MHPs with sizeable spin-polarized photoluminescence [30], and even proposed metal-free 3D bulk chiral MHPs [31]. Notably, Ma et al. demonstrated 2D chiral MHPs microplates with g_{PL} as high as ≈0.35 at 77 K [32]. Building on these materials advances, chiral 2D MHPs have recently been integrated as spin-filtering layers in room-temperature spin-LEDs, as demonstrated by Kim et al. in 2021 using $(R/S\text{-MBA})_2PbI_4$ CISS layers coupled to $CsPbI_3$ nanocrystal emitters [33]. More recently, He et al. realized MHPs spin-LEDs based on chiral $CsPbBr_3$ quantum dots that combine large electroluminescence dissymmetry ($g_{EL} \approx 0.3$) with EQEs up to 16.8% [34], highlighting the need for future efforts toward lead-free compositions, long-term operational stability, and extended spin lifetimes.

As an emerging field, recent advances in chiral MHP synthesis, materials chemistry, and potential for CPL have been reviewed elsewhere [15, 35, 36, 19, 37]. In this Perspective, we focus specifically on chiral MHP spin-LEDs and compare two device concepts, i.e., intrinsic chiral emitters and extrinsic spin-filtered architectures, analyzing and highlighting how materials design, device structure, and interfacial spin transport govern CPL performance. We discuss key challenges for moving from filter-based CP light sources to robust, source-level polarization.

2 | Fundamental Origin of Chirality and Spin Polarization in MHPs

Before exploring the mechanisms operative in LEDs, it is essential to understand how chirality is introduced into MHPs and how it influences their electronic structure through symmetry breaking and SOC. In this section, the key structural distortions that govern chirality transfer and spin selectivity are discussed. From a molecular perspective, varying the structure of the chiral organic cations can lead to varying degrees of asymmetric hydrogen bonding with the inorganic framework, which significantly affects the resulting chiroptical properties [38]. Strategies for tuning the molecular design of chiral cations include: 1) Introducing extended π–π stacking by incorporating large π-conjugated systems such as a naphthalene skeleton (e.g., *R/S*-NEA) [39]. 2) Promoting halogen-based interactions, including halogen–halogen intermolecular interactions between halogen-substituted chiral cations and the inorganic layers (e.g., *R/S*-MBA-X, X = F, Cl, Br, I) [35, 40], and modulating the substituents on aromatic ammonium

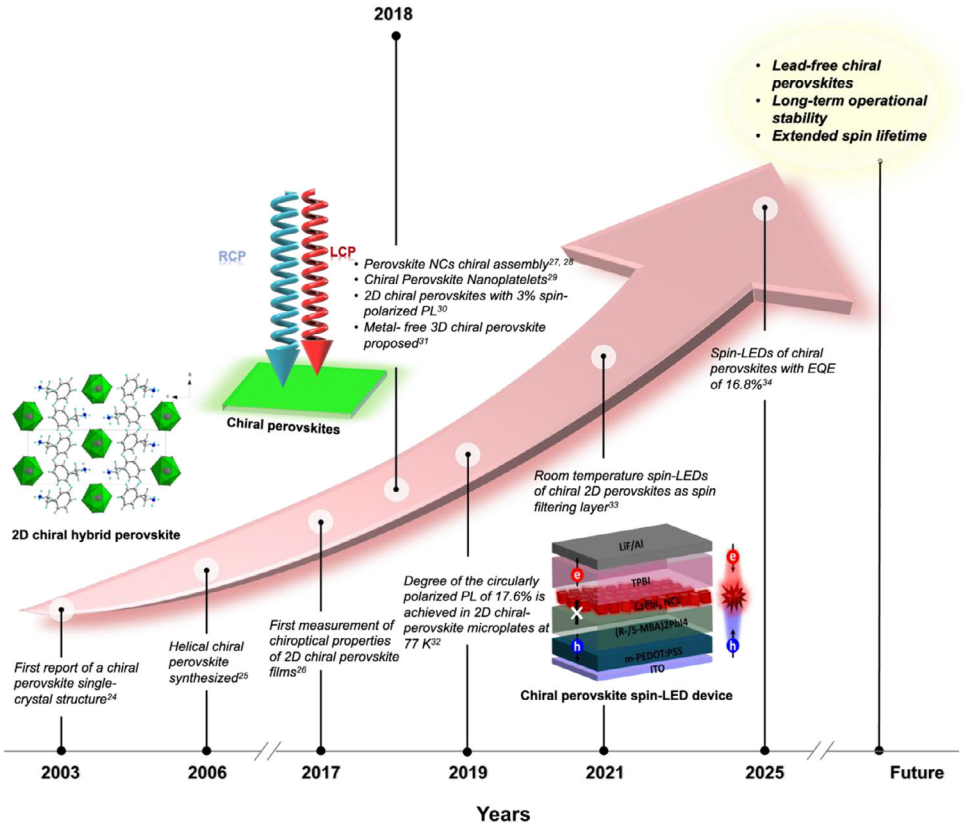

FIGURE 2 | Timeline of key milestones in chiral MHPs research, from the first crystal structure report to recent demonstrations of spin-LEDs. Future directions may include lead-free chiral MHPs, long-term operational stability, and extended spin lifetimes.

cations [41]. 3) Inducing CH···π interactions by using mixed chiral–achiral cation systems (e.g., comprising a blend of chiral ammonium and achiral alkylammonium spacer cations) [42–44]. For example, stronger intermolecular π–π interactions between chiral cations helps to align the ligands, which in turn facilitates a uniform and organized asymmetric distortion of the inorganic framework, enhancing the system's overall chiroptical properties.

The chirality transfer in chiral MHPs is suggested to occur through the following mechanisms: (i) chiral templating of the surface through structural distortions, (ii) formation of a chiral supercell via the geometric pattern of achiral cations [45], (iii) chiral molecular dipole–MHPs transition dipole coupling [46], and (iv) creation of a chiral crystal structure (i.e., Sohncke chiral space group) [19]. In addition, a recent study has reported that MHP NCs with unequal basal edge lengths can have chiral symmetry C1, resulting in a CD peak, even though bulk ferroelectric $CsPbBr_3$ is non-chiral [47].

Chiral templating of the surface via structural distortions or twisted assemblies involves chiral cation ligands (small molecules or polymers) attached to the surface of MHP NCs [27, 48]. These surface ligands induce an asymmetric distortion of the local lattice or forms twisted NC assemblies [49], transferring chirality to the NCs. However, the first effect is largely confined to the surface region and does not propagate through the bulk of the perovskite lattice. Consequently, although chiral MHP NCs can be successfully synthesized using this approach, the efficiency of chirality transfer is inherently limited to the surface. A similar limitation applies to chiral molecular dipole–perovskite transition dipole coupling [46]. In this case, the origin of chirality transfer is the interaction between the static molecular dipoles of the molecular enantiomers and the transition dipoles at the cluster surface of the perovskite. Since the coupling is restricted to the surface dipoles, the induced chirality does not extend throughout the perovskite lattice. On the other hand, the twisted assemblies exhibit higher dissymmetry factors due to strong light-matter interactions [49]. In contrast, formation of a chiral supercell via the geometric arrangement of achiral cations or creation of a chiral crystal structure induces asymmetric distortions throughout the entire inorganic framework [45]. These approaches generate more coherent and pronounced chirality because the distortion is not confined to the surface but is propagated across the bulk structure. Accordingly, current evidence suggests that strategies promoting highly ordered, coherent asymmetric distortions throughout the bulk lattice are the most effective for achieving strong chirality in perovskite materials.

Importantly, electrical excitation of a chiral MHP emitter can give rise to CP-EL. Alternatively, CP-EL can be generated (even in achiral emitters) from the injection of spin polarized charge carriers. In principle, the higher the spin polarization of the carriers, the greater the anisotropy of the CPL emission, while also reducing spin-mismatched recombination pathways. As such, the generation of spin polarized carriers can not only allow for CP-EL, but also improve charge carrier dynamics, LED lifetime, and internal quantum efficiency (IQE). For chiral MHP interlayers, spin polarization is generated via the CISS mechanism. Since the first discovery of the CISS effect in typical chiral 2D MHPs ($(R/S\text{-MBA})_2PbI_4$ (R/S-MBA = R/S-methylbenzylamine) [50], a variety

of chiral MHPs have been reported to show CISS by measuring magnetic conductive-probe atomic force microscopy (mc-AFM) [51–59].

The crystal structures of chiral MHPs used for the spin filtering and their P_{spin}, dissymmetry factor of circular dichroism (g_{CD}), and distortion index (D) are summarized in Figure 3a–i. It is noteworthy that the chiral MHPs incorporating chiral organic cations with stronger intermolecular interactions, especially for π–π interactions, tend to produce a more pronounced CISS effect. For example, MBA- and NEA-based chiral MHPs exhibit the higher P_{spin}, while alkyl chain-based chiral molecules (e.g., HP1A, PRDA, BA), which lack π–π interaction groups, show the lower P_{spin}. Furthermore, a stronger CISS effect often is accompanied by enhanced circular dichroism (CD), suggesting that the P_{spin} may correlate with chiroptical properties (g_{CD}) (Figure 3i). For example, alloying $(PEA)_x(S\text{-}PRDA)_{2-x}PbBr_4$ with a small amount of Sn (10%) resulted in a significant amplification of g_{CD}, leading to a higher P_{spin} of 84%, compared to 60% for the pure Pb-based composition, attributed to the larger degree of octahedral bond distortion compared to the pure Pb-based counterpart [60].

Despite such correlations, the precise origins and key factors that contribute to the strong CISS effect in chiral MHPs require further investigation. Further studies are needed to better understand the relationship between chiroptical properties, SOC, molecular design of chiral MHPs, and the CISS effect. As the CISS effect is often accompanied with a high D, this may indicate that D could be an important factor influencing CISS anisotropy. D is defined as: $D = \frac{1}{6}\sum_{i=1}^{6}\frac{|d_i - d_0|}{d_0}$, where d_i represents the individual metal–halide bond lengths, and d_0 is the average metal–halide bond distance. In an ideal octahedron, D would be zero. While greater lattice distortion can enhance chiroptical activity, Babu et al. demonstrated that pronounced CD responses can also occur when $D = 0$, highlighting that electronic asymmetry and chiral molecular interactions, rather than just geometric distortions, can govern chiroptical and spin-dependent behavior [61]. However, D does not exhibit a clear correlation with the P_{spin}.

3 | Mechanism-Based Classification of Spin-LED Architectures

In principle, two primary device architectures have been explored to realize CP-EL in chiral MHPs-based spin-LEDs, as seen in Figure 4. The first approach employs intrinsically chiral emitters. In this approach, the chirality and emission both derive from the active layer, and the resulting polarization originates from asymmetric electronic transitions that are controlled by the chiral potential and Rashba-type band splitting. The second pathway is via selective spin-pumping, whereby circular polarization is realized extrinsically by injecting spin-polarized carriers into an achiral emissive layer. Here, the spin-selective transport is either mediated through the CISS effect or ferromagnetic contacts to provide spin-polarized electrons and holes, which radiatively recombine to emit CPL. While both mechanisms exploit the SOC-structural asymmetry coupling, they fundamentally differ in the mode of action. Figure 4 illustrates the two device architectures and their working mechanisms of MHPs spin-LEDs, i.e., intrinsic and extrinsic. Table 1 summarizes the key distinguishing features of these two mechanisms that are critical for the operation of spin-LED devices. In the subsequent sections, we examine how both strategies have been realized across various chiral MHPs systems, with particular emphasis on the underlying material design principles, device architectures, and their resulting performance metrics for spin-LED application.

3.1 | Intrinsic Chiral Emitters (Chiral Emission Zone)

In these systems, the optical polarization stems from the intrinsic electronic structure of the chiral MHPs, where symmetry breaking within the lattice couples with strong spin–orbit interactions to produce spin-split energy bands and spin-selective radiative recombination pathways [63]. The magnitude of the Rashba splitting, which is determined by the extent of lattice distortion and SOC strength, is a key parameter [64]. While intrinsic spin-split bands facilitate efficient CPL emission without the use of external spin filters, translating this intrinsic mechanism into high-performance devices requires a careful design strategy. The same lattice distortions that strengthen chirality and Rashba splitting can also generate trap states and impede carrier mobility, leading to nonradiative losses and lower EL efficiency. Therefore, an optimal spin-LED architecture must balance chiral asymmetry to maintain strong polarization with electronic transport characteristics that ensure efficient light emission.

3.1.1 | 2D and Quasi-2D Chiral Emissive Films

2D and quasi-2D MHPs have attracted significant attention as promising intrinsic chiral emitters, as their layered structures facilitate stronger SOC and tighter exciton confinement [65, 66]. The interplay between octahedral distortions and the layered organic–inorganic structure in 2D MHPs allows for additional modulation of asymmetry, which promotes more efficient chirality transfer from the organic spacers to the inorganic Pb–X octahedra [64, 67]. Also, the in-plane variation in the bond angles in non-centrosymmetric systems influences the spin splitting. An increase in tilting asymmetry (Pb-X-Pb) leads to greater inversion asymmetry within the inorganic layer, resulting in enhanced spin splitting [68]. In MHPs, the combination of inversion-symmetry breaking and strong SOC generates Rashba-split bands with momentum-dependent spin helicities, such that radiative recombination is favored between electrons and holes that occupy Rashba branches with aligned spin helicity, while transitions between opposite-helicity states are suppressed. This helicity-selective recombination results in intrinsically circularly polarized emission. Consequently, tuning the bond angle (Pb-X-Pb), for instance by tuning the organic spacer size or halide composition, is crucial for maximizing spin polarization and the EL dissymmetry. For instance, pure organic/inorganic MHPs based on methylammonium (MA) or formamidinium (FA)- systems have shown similar spin-lifetime which indicates a minimal effect of A-site cation, whereas the variation of halogen ions along with inorganic sublattice have shown significant impact on spin transport behavior [69]. Beyond static structural factors, Rashba splitting in 2D and quasi-2D perovskites is influenced by external electric fields and temperature, making it a dynamic rather than fixed electronic property. For instance, both first principles

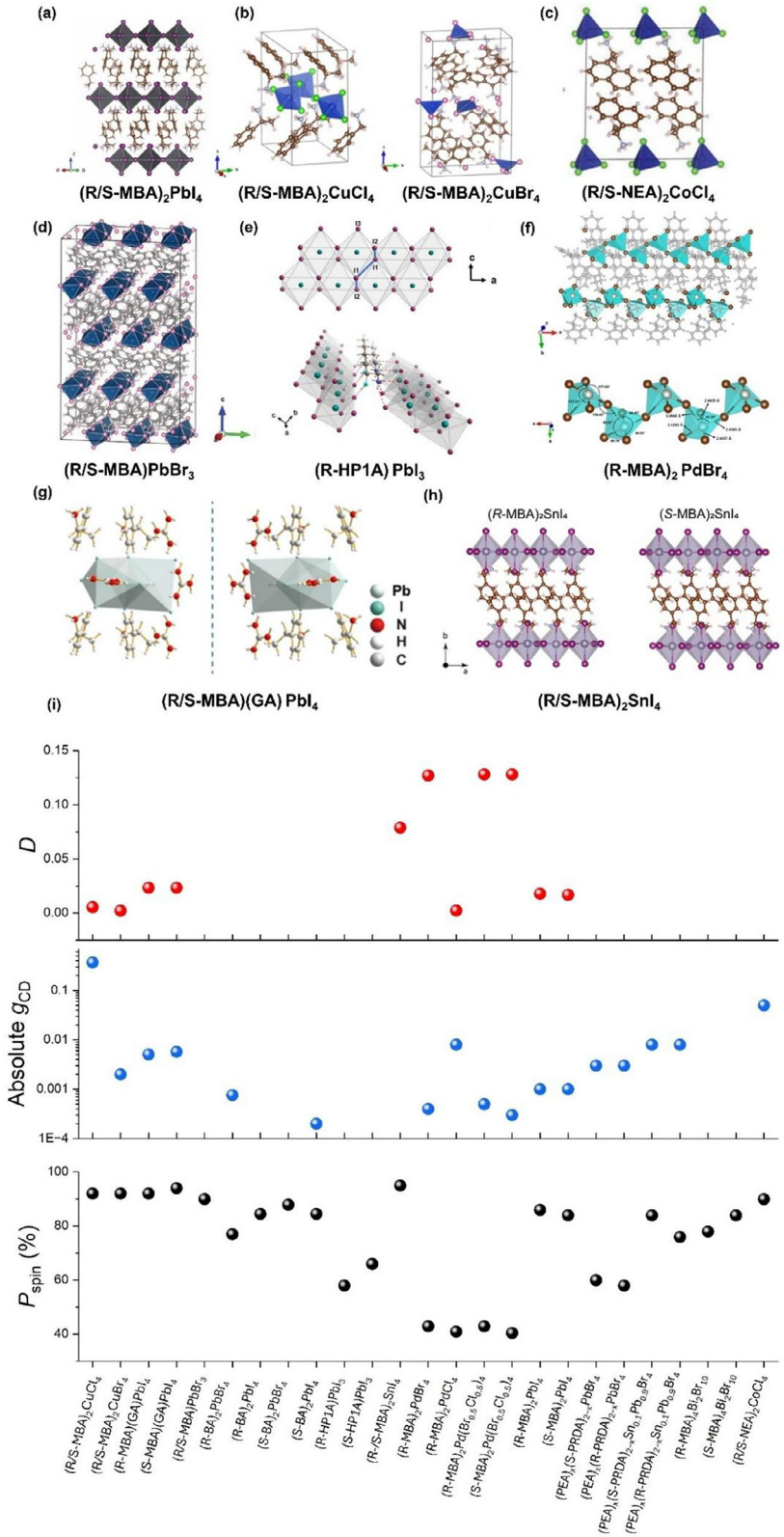

FIGURE 3 | Reported chiral MHPs used for spin polarization and their D, $g_{CD,}$ and P_{spin}. Crystal structures of a) (*R/S*-MBA)$_2$PbI$_4$, b) (*R/S*-MBA)$_2$CuCl$_4$ (left) and (*R/S*-MBA)$_2$CuBr$_4$ (right), c) (*R/S*-NEA)$_2$CoCl, d) (*R/S*-MBA)PbBr$_3$, e) (*R*-HP1A)PbI$_3$, f) (*R*-MBA)$_2$PdBr$_4$, g) (*R/S*-MBA)(GA)PbI$_4$, h) (*R/S*-MBA)$_2$SnI$_4$, and their i) D (top), g_{CD} (middle), and P_{spin} (bottom) [51–56, 60, 62].

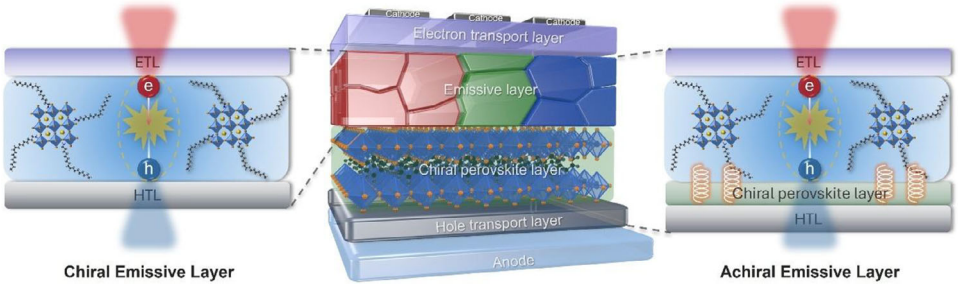

FIGURE 4 | Schematic illustration of two distinct emission mechanism in chiral MHPs spin-LEDs and the resulting (CP-EL) process. a) Intrinsic mechanism: circularly polarized emission originates directly from a chiral emissive layer, Extrinsic mechanism: CP-EL arises through spin-pumping, in which spin-polarized carriers are generated in a CISS-active chiral spin-filter layer and injected into an achiral emissive layer.

TABLE 1 | Comparisons of key material characteristics, device architectures, and performance aspects of intrinsic and extrinsic emitter for chiral MHPs-based spin-LEDs.

Key aspect	Intrinsic chiral emitter LED	Extrinsic Spin-pumping LED
Polarization route	Intrinsic to emissive material (chiral lattice with asymmetric recombination)	Extrinsic via spin-polarized carrier injection via CISS or magnetic interface
Material Type	Chiral MHPs, chiral organics, or helicene-functional QDs	Chiral MHPs spin-filters + achiral emissive layer such as QDs
Crucial Factors	Chirality strength and dimensionality	Spin polarization efficiency
Spin dynamics	Spin splitting promotes intrinsic spin polarization and asymmetric recombination. Influences g_{EL}	Spin splitting governs spin-injection efficiency and spin-filter selectivity. Influences P_{inj}
Spin lifetime	Governs spin preservation before radiative recombination. Higher lifetime can result in higher CPL	Determines spin diffusion length and spin preservation while crossing through interface.
EQE (%)	Higher in optimized 2D/3D heterostructure	Lower due to interfacial losses
Dissymmetry factor g_{EL}	10^{-3}–10^{-1}	10^{-4}–10^{-1}
Advantages	Simple device design and Integration	Independent optimization of spin generation and emissive layer
Challenges	Achieving simultaneously higher g_{EL} and EQE	Effective spin injection and depolarization at interfaces

calculations and experimental studies have shown that an applied or built-in electric field can significantly alter the Rashba splitting energy (E_R) and coefficient (α_R) by modifying lattice distortion, surface ligands, interfacial dipoles, and flexibility of the inorganic framework, thereby dynamically tuning spin textures under device-relevant bias conditions [70]. Moreover, while thermal broadening generally promotes spin-phonon scattering and spin dephasing, as temperature dependent measurements indicate that thermally activated octahedral distortions and polar fluctuations can, in some cases, strengthen Rashba splitting at higher temperature. Recent work further demonstrates that both the magnitude and thermal evolution of Rashba splitting are highly sensitive to organic spacer polarity and exciton-phonon coupling, highlighting the role of lattice softness and dynamic disorder in governing spin-split excitonic states [71, 67].

Apart from intrinsic properties and externally tunable electronic states, designing single layer spin-LEDs with higher PLQY and strong optical chirality based on chiral MHPs emissive layer remains a challenge due to competing electronic and structural constraints. Recently, Yang et al. reported the link between chiral organic spacers, lattice distortion and spin–orbit fields to realize spin-polarized emission. The group designed a single layer spin-LEDs based on quasi-2D MHPs with achiral phenethylammonium iodide (PEAI) and chiral *S*/*R*-1-(1-naphthyl)ethylammonium iodide (*S*/*R*-NEAI) as dual spacer cations within a RP lattice. The presence of chiral cation broke the inversion symmetry and induced strong Rashba-type band splitting in the emissive layers. In a further step, the amalgamation of PEAI and NEAI, combined with in situ passivation using carbazole-functionalized phosphonium [(9-ethyl-9H-carbazol-3-yl)triphenylphosphonium iodide, TPPCzEtI], resulted in smoother film morphology and narrower emission peaks. This engineering yielded stable spin-LEDs with g_{PL} and g_{EL} values of 2×10^{-3} and 4×10^{-3}, respectively, and an EQE approaching 3.7% [72]. The same group later introduced an in-situ ligand-engineering strategy using chiral binaphthyl ligands (*R*/*S*-BinapO) to modify $MAPbBr_3$ NCs [73]. These chiral ligands

simultaneously passivated defects and imposed chiral distortion within the MHPs lattice, which resulted in a lower g_{PL} of 5.6 $\times 10^{-3}$. The measured CPL from the device was higher (g_{EL} of 1.8 $\times 10^{-1}$), the highest reported for a single-layer chiral MHPs LED at the time. PLQY also enhanced from 0.9% to 37.9% after chiral passivation. The simplicity of the device design, requiring no additional spin-injection layer, underscored the promise of lattice-embedded chirality for achieving both efficiency and polarization.

On the other hand, Yao et al. demonstrated green LEDs based on quasi-2D chiral MHPs(*R/S*-$NEA_2(FA_{0.85}Cs_{0.15})_2Pb_3Br_{10}$). The optimized chiral MHPs thin film demonstrated a strong CPL at 535 nm with a near unity PLQY of 91%, and g_{PL} of 8.6 $\times 10^{-2}$. The designed spin-LED exhibited self-contained spin and energy funneling within the same emissive film, and ultrafast transient spectroscopy revealed the presence of long-lived excitons from sub-picosecond (0.2 ps) transfer of spin-polarized excitons from 2D chiral domains to 3D emissive regions, leading to g_{EL} around 7.8 $\times 10^{-2}$, and EQE of 13.5%, as shown in Figure 5a–f [74].

Dual-ligand and interfacial strategies further illustrate how chirality transfer and radiative efficiency can be co-optimized in quasi-2D emissive films. Yan et al. showed that mixed-ligand quasi-2D perovskites can switch from transfer-type CP emission to an intrinsic regime: when the lowest-bandgap emitting phase itself exhibits intrinsic chirality, CP-EL arises from direct recombination within that chiral emissive phase, enabling standard and deep-blue CP-LEDs with g_{EL} up to 1.75 $\times 10^{-1}$ [75]. Jiang et al. employed a chiral hybrid MHP emitter (*R/S*-p-$FMBA)_2Cs_1FA_1Pb_3I_{10}$ together with a MeO-2PACz self-assembled monolayer at the HTL/MHPs interface, improving film quality, suppressing ion migration, and extending the spin lifetime, which led to red spin-LEDs with EQE of 8.3% and g_{EL} of 1.6 $\times 10^{-1}$ [76]. Zhang et al. used chiral ionic liquids during quasi-2D film formation to simultaneously imprint chirality and passivate defects, obtaining sky-blue devices (491 nm) with $g_{EL} \approx$ (1.3–1.6) $\times 10^{-1}$ and EQE of 13% [77].

3.1.2 | Intrinsic Nanostructured Emitters

Beyond 2D and quasi-2D chiral MHPs, recent work has extended intrinsic chirality to colloidal NCs by engineering surface ligands and ionic environments. Chen et al. demonstrated in-situ high-temperature modification of $CsPbBr_3$ NCs with chiral *R/S*-bPEABr ligands, imprinting chirality directly onto the NC surface without forming low-dimensional phases. The resulting chiral emitters combined a high PLQY of ≈ 89% with an impressive EQE of 15.4% and CP-EL with $g_{EL} \approx 2.2 \times 10^{-3}$ at room temperature, establishing NC-based intrinsic chiral emitters as competitive with 2D systems in LED devices [21].

Further developments have explored materials chemistry, orientation and interfacial effects as routes to boost the performance of chiral emitters. In one such approach, chirality and light emission are combined within host–guest structures. Ren et al. embedded $CsPbBr_3$ NCs into the helical channels of enantiomeric metal–organic frameworks (*L*/*D*-MOFs, Figure 5g–m), where the chiral scaffold imposes helical ordering and Cd–Br coordination at the interface, transferring chirality into the achiral MHPs lattice. Simultaneously, the blue-emitting MOF host acts as a Förster resonance energy transfer (FRET) donor that funnels excitation into the NCs, yielding a PLQY of 78% and $g_{PL} \approx 8.4 \times 10^{-3}$ and enabling CP white LEDs with luminous efficiency of 68.6 lm W^{-1} and good operational stability, showing no spectral variation even after 2 hours of continuous operation [78].

Low-dimensional MHPs NCs such as ultrathin nanowires (NWs) and nanoplatelets (NPLs) also exhibit CPL when combined with chiral ligands, with several studies highlighting the impact of monolayer thickness and superlattice orientation on CPL performance. Chen et al. recently extended this concept to all-inorganic chiral $CsPbX_3$ ultrathin NWs, where chirality originates intrinsically from helical lattice distortion caused by chiral ligands. Interestingly, the handedness of the NWs was precisely controlled using very small concentrations of chiral amines (e.g., *R/S*-MBA), which do not bind strongly to the crystal surface, but guide symmetry breaking in NWs. Room-temperature synthesis of left- and right-handed ultrathin NWs (<2 nm diameter) was demonstrated, exhibiting both CISS-driven spin selectivity and CP-EL (g_{EL} of 5×10^{-3}) [79]. Cao et al. reported an inverse relation between NPL thickness and CPL/CD strength, while Wang et al. used a solvent-mediated post-synthetic treatment to imprint chirality in $CsPbBr_3$ NPLs via simultaneous chiral ammonium ligand exchange and partial B-site cation exchange [80]. In these systems, enhanced CPL was attributed to ligand-induced lattice distortions and exciton delocalization across ordered stacks, which strengthens magnetic-dipole transition matrix elements.

3.2 | Extrinsic Spin-Injection Devices (Achiral Emission Zone)

Extrinsic spin-LEDs build on concepts from semiconductor spintronics. They achieve CP-EL by injecting spin-polarized carriers from a chiral CISS-based spin-filter layer into an achiral emitter (Figure 4a), thereby decoupling spin selection from light generation. As such, the emissive layer can remain achiral, enabling the use of high-PLQY MHPs NCs or quantum wells while maintaining significant polarization output. The radiative recombination of spin-polarized carriers follows angular momentum conservation rules ($\Delta m_j = \pm 1$), resulting in preferential left- or right-handed photon emission, depending on the handedness of the chiral medium. g_{EL} in such devices depends on the spin polarization efficiency (P_{inj}), spin coherence lifetime (τ_s) and spin-preserving recombination probability. Therefore, two key requirements must be satisfied for high-performance spin-LEDs via this mechanism: (i) efficient spin-polarized carrier injection and transport [33], and (ii) an emissive MHPs that maintains a high PLQY while preserving spin coherence [81].

The physics of the CISS effect has been widely reviewed elsewhere [82]. In currently reported device architectures, low-dimensional chiral MHPs are employed as spin-selective layer. They are positioned between the charge transport layer and an achiral MHPs emitter layer. The steric hindrance of the chiral spacer molecules can inhibit the crystallization of 2D chiral MHPs, resulting in enhanced structural defects [83]. Consequently, carrier losses often occur during charge transport or across the additional interface separating the chiral and achiral MHPs layer. Additionally, there is a high probability of spin relaxation of

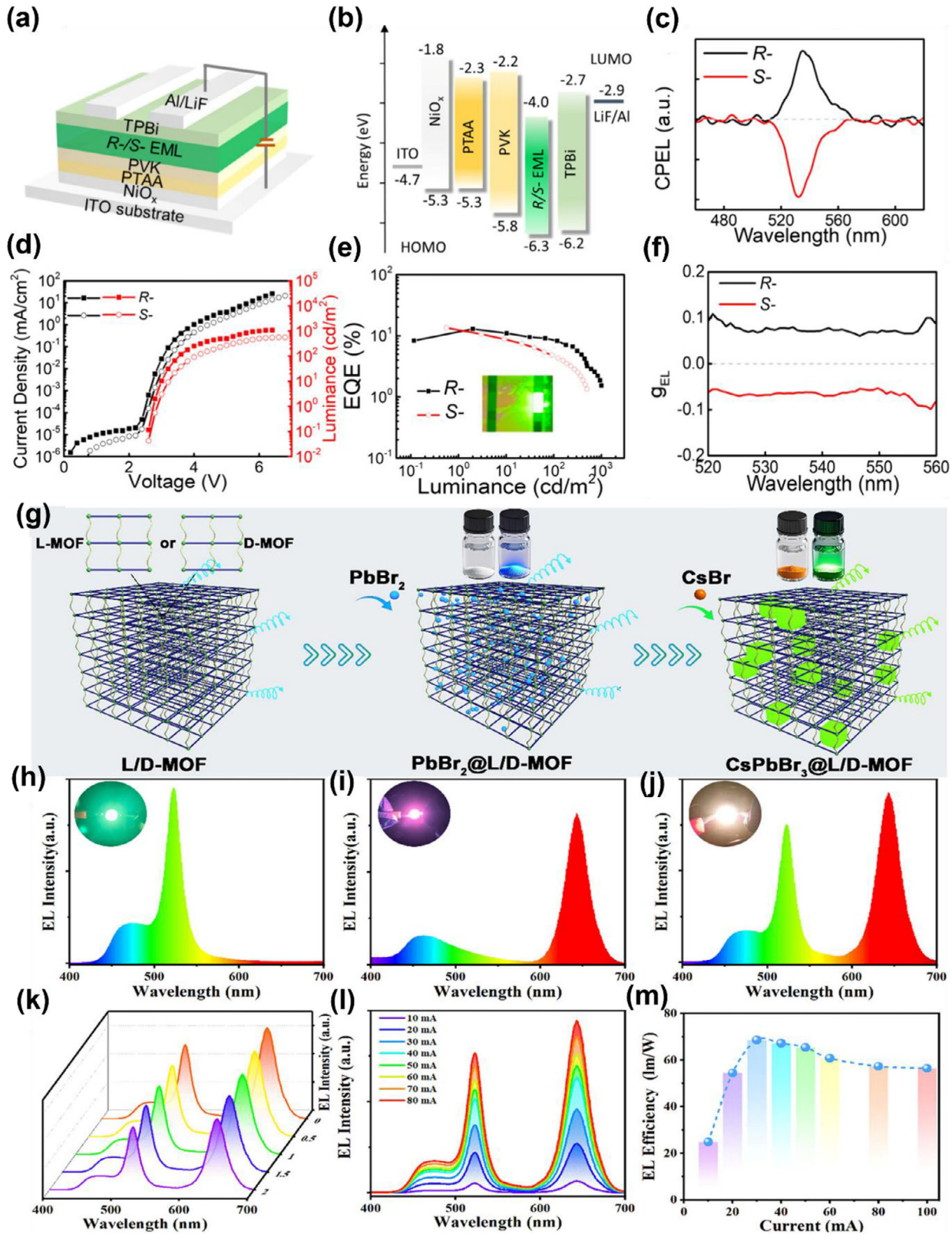

FIGURE 5 | Structure and performance of spin-LEDs based on *R/S*-$NEA_2(FA_{0.85}Cs_{0.15})_2Pb_3Br_{10}$ as an emitting layer: a) device structure, b) energy level bandgap diagram of different layers, c) CP-EL, d) current density–luminance–voltage (J–L–V) curves, e) EQE–luminance curves, f) Left- (σ^+) and right-hand (σ^-) CP-EL spectra of spin-LEDs based on *R*-$NEA_2(FA_{0.85}Cs0.15)_2Pb_3Br_{10}$. Reproduced with permission from Ref. [74]. Copyright 2024, American Chemical Society. g) Schematic illustration of the synthesis of $CsPbBr_3$@L/D-MOF composites, h) emission spectra and photographs of $CsPbBr_3$@D-MOF-based green LED, i) $CsPbBrI_2$@D-MOF-based red LED, j) $CsPbX_3$@D-MOF based white LED, k) Long-term operating test of $CsPbX_3$@D-MOF-based white LED, l) EL intensity, and m) EL efficiency of $CsPbX_3$@D-MOF-based white LED at different operating currents. Reproduced with permission from Ref. [78]. Copyright 2025, Wiley-VCH GmbH.

the spin-polarized carriers before radiative recombination in the achiral MHPs layer.

To address the above-mentioned challenges, researchers have explored modulating the chiral MHPs structure in order to suppress non-radiative routes and enhance both spin preservation and carrier injection efficiency, resulting in an improved performance of CISS-based spin-LEDs. To date, there are three primary design strategies which have been explored, including: a) layered heterostructures, b) mixed-phase or quasi-2D architectures for inter-phase spin transfer, and c) hybrid dual-function chiral NCs or NWs.

3.2.1 | Bilayer Spin-Filter Heterostructures

Important initial work by Kim et al. demonstrated a CISS effect-based spin-LED where 2D chiral (R/S-MBA)$_2$PbI$_4$ acted as a spin-filter layer, injecting spin-polarized carriers into achiral CsPb(Br$_{1-x}$I$_x$)$_3$ QDs, which resulted in a g_{EL} of 5.2×10^{-2} that operates at room temperature without magnetic fields or ferromagnetic contacts. This laid the foundation to use layered heterostructure for spin-LEDs, in which 2D chiral and 3D achiral materials are used as a spin filter and an emissive layer, respectively [33]. Using a similar concept, Ye et al. developed type-II core–shell NCs with a low-dimensional chiral MHPs shell and achiral 3D MAPbBr$_3$ core. The shell injects spin-polarized carriers into the core via the CISS effect, resulting in CPL emission from the core. Notably, the transfer of valence band electrons through the chiral MHPs shell occurs in a spin-dependent manner, leading to a spin-polarized distribution of holes in the valence band of the achiral core spin-LEDs fabricated from these core–shell structures resulted in CP-EL with a g_{EL} of 6×10^{-3} [20]. Similarly, core–shell MHPs quantum dots (PQDs) were tested for spin-LEDs, where a 2D chiral MHPs ((*R*)-and(*S*)-1-(2-(naphthyl)ethylamine)(*R/S*-NEA)) shell is deposited onto an achiral 3D inorganic MHPs core (CsPbBr$_3$). The 2D chiral cations were found to passivate the halide vacancies at the surface of the PQDs, which resulted in a higher PLQY of 78% as compared to 71% of core PQDs, and the resulting spin-LED exhibited an EQE of 5.5%.

Importantly, in layered and core-shell spin-LED architectures, bringing together a 2D chiral spin filter and 3D achiral emissive layer can naturally introduce lattice mismatch and interfacial strain due to difference in dimensionality, lattice constant, octahedral connectivity, and organic–inorganic bonding motifs. Slight modulation in interfacial distortion can be beneficial, as it enhances local inversion asymmetry and Rashba-type spin splitting, thereby improving spin selectivity at the interface [68, 84]. However, excessive mismatch might lead to dislocations, surface defects, and trap states that can accelerate non-radiative recombination and spin dephasing, resulting in lowering both g_{EL} and EQE. Furthermore, the built-in electric field associated with strained heterointerfaces can alter band alignment between the emissive layer and charge transport layer, as well as the local Rashba coefficient, affecting spin injection and transport under operating bias. Mitigating these competing effects while preserving efficient spin injection requires careful interfacial engineering [85, 86]. Strategies such as a) inserting graded quasi-2D transition layer where the variation in n enhances carrier mobility, and significantly extend spin lifetime [87], or quasi-2D transition layer with intermediate lattice constants to reduce mismatch, b) optimizing the thickness and composition of chiral layer to balance spin filtering and carrier tunneling, c) employing surface passivation or flexible organic spacers to suppress defect formation, d) tuning interfacial dipole and band offsets to maintain efficient spin-polarized carrier transfer, and e) exploring interfacial chirality-induced growth at the heterostructure interface [88].

Moreover, apart from core-shell design, dimensionality and doping can also influence the CISS effect for efficient spin transfer, as mentioned above [89]. For instance, Feng et al. reported enhanced CISS effect by tuning the A-site and B-site mixed cation for a green emissive spin-LED. The 2D chiral MHPs (PEA)$_x$(S/R-PRDA)$_{2-x}$Sn$_{0.1}$Pb$_{0.9}$Br$_4$ was employed as the CISS layer, exhibiting elevated CISS effects with stated spin polarization exceeding 80%. This material was used alongside achiral CsPbBr$_3$ NCs and resulted in spin-LED with an EQE of 5.7%, and g_{EL} of 1.1×10^{-3} (Figure 6a–f) [58].

3.2.2 | Mixed-Phase Quasi-2D "Internal Heterostructures"

Unlike layered heterostructures, which mostly utilize 2D chiral MHPs with an adjacent 3D achiral emissive layer, mixed-phase or quasi-2D systems use chiral and achiral MHPs phases that coexist within a single film. Although fabricated as a single mixed-phase film, these devices are "extrinsic-like" functionally because spin selectivity is established in the chiral low-n domain, while EL predominantly originates from the higher-n (effectively achiral) emissive domain. Such structures enable ultrafast energy and spin funneling across internal interfaces, and this intrinsic heterogeneity might be beneficial for enhancing spin injection efficiency and minimizing carrier losses. For instance, Zhang et al. designed a quasi-2D MHPs spin-LED using mixed chiral-achiral spacers for the CISS effect rather than relying only on a chiral cation. Specifically, they combined chiral (R/S-MBA) and achiral *tert*-butylammonium (*t*-BA), forming a band-II heterojunction between the chiral $n = 1$ QW and the achiral higher-n QW. This resulted in hole back-transfer and interphase spin filtering via the CISS effect. The incorporation of the achiral spacer not only promoted the formation of higher-n QWs but also randomized the orientation of the chiral lower-n QWs, forming a vertically uniform distribution that promoted spin-polarized carrier tunneling within a single MHPs layer [90]. In another approach, R/S-MBA and 2PEA were co-employed as dual ligands to achieve blue-emissive quasi-2D spin-LEDs with 3.8% EQE and 93% stated spin polarization [91]. In another report, Li et al. [92] devised a spin-LED architecture utilizing high-quality chiral quasi-2D MHPs that enabled spin-polarized charge recombination and CP-EL, without requiring a heterojunction of distinct functional materials. Their design employed an ultra-thin ($n = 1$) bottom layer serving as a spin-filtering interface, while a quasi-2D MHPs ($n = 3$) acted as the recombination and emission center. This device achieved a $g_{EL} \approx 1 \times 10^{-1}$, attributed to the emission-chiral vertical stacking configuration of the MHPs layers. Notably, a spin carrier lifetime of 20 ps was reported. The overall final device exhibited an improved EQE of 15.4%. Similarly, using a chiral quasi-2D MHPs together with different halide compositions, Yao et al. reported spin-LEDs with emission wavelengths tunable from red

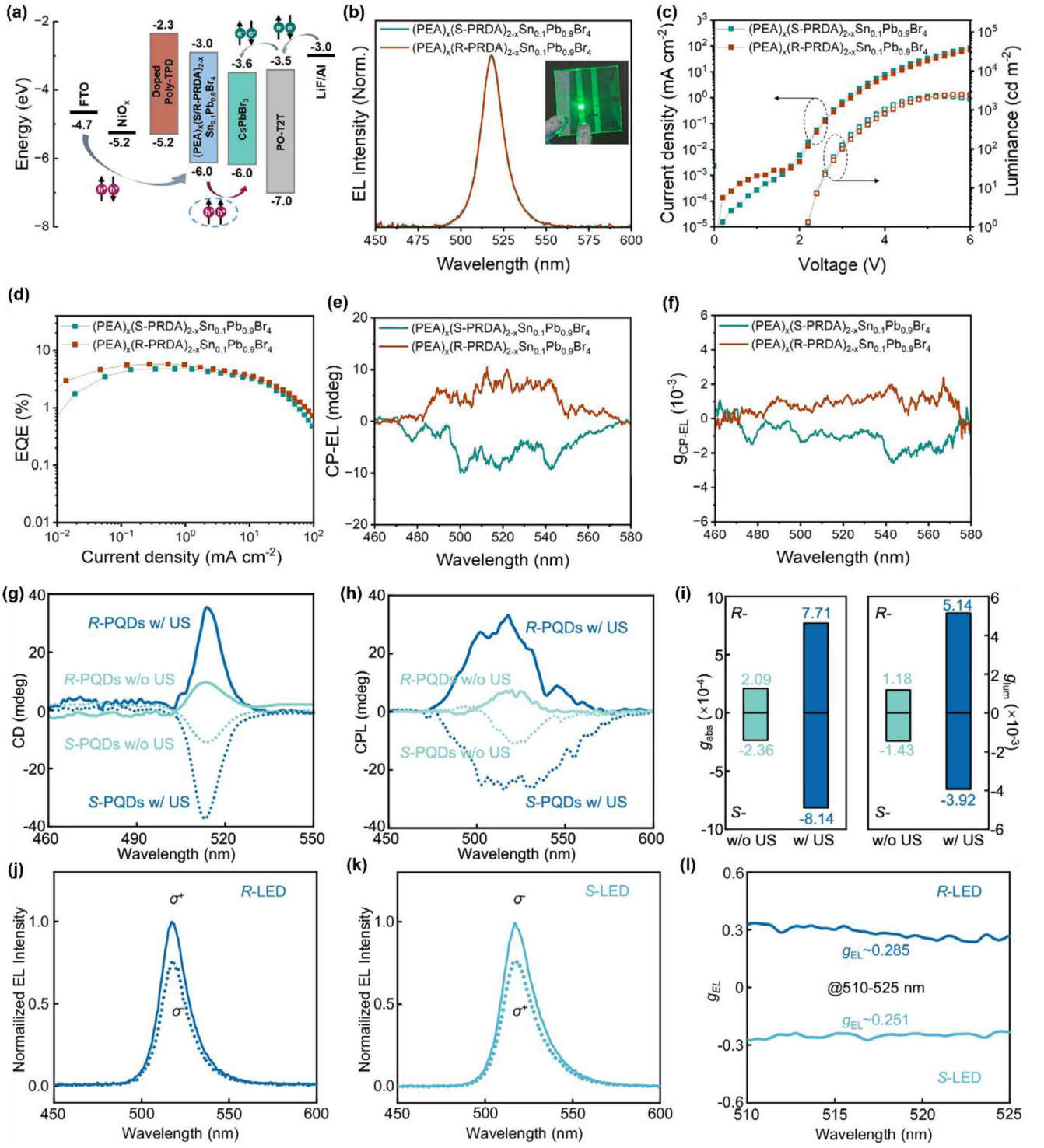

FIGURE 6 | Performance of spin-LEDs. a) The energy level diagram for the spin-LEDs made of the different layers. The complete structure is ITO(glass)/m-PEDOT:PSS/quasi-2D MHPs/TPBi/LiF/Al structure, b) Bias voltage dependent electroluminescence spectra for the *R*-CHP based spin-LEDs, c) Current density–voltage–luminescence (*J–V–L*) characteristic curves for the *R-/S*-CHP based spin-LEDs, d) Measurements of EQE current density curves for spin-LEDs with optimal performance, e) Derived dissymmetry factor (g_{EL}) for the *R-/S*-CHP based spin-LEDs, f) The cross-sectional scanning electron microscopic image for the spin-LED comprising ITO/m-PEDOT:PSS/CHP/TPBi/LiF/Al. Reproduced with permission from [58]. Copyright 2024, American Chemical Society, and g) CD and h) CPL spectra of chiral $CsPbBr_3$ PQDs with different ligand exchanged processes. US ultrasonic treatment. The corresponding i) g_{abs} and g_{PL} values of chiral $CsPbBr_3$ PQDs with different ligand exchange processes, j) *R*-LED, k) *S*-LED, l) Wavelength-dependent g_{EL} of *R/S*-LEDs. Reproduced under the terms of the CC-BY license [34]. Copyright 2025, The Authors.

(675 nm) to near-infrared (788 nm). The rational design of *R/S*-$NEA_2(FA_{0.8}MA_{0.2})_2Pb_3Br_{10-x}I_x$ MHPs, combined with the incorporation of a phosphoric acid-based additive (EDTMP), enabled not only emission tuning but also significant defect passivation and improved film morphology. This led to an impressive PLQY of 86.7% and an EQE of 12.4%. Given that the g-factor of CPL is closely related to the ratio of τ_{spin} to τ_{rad}, iodide-rich chiral MHPs, featuring longer spin coherence times and shorter radiative lifetimes, exhibited enhanced CP-EL responses [93]. For example, an increase in iodide content has g_{EL} values reaching as high as 1.48×10^{-2}.

To further deepen the understanding of spin-related chiroptical performance such as spin lifetime, magnetic transition dipole moment and chiral-induced spin orbit coupling (CISOC) and the impact of temperature on g-factor of circular polarization in quasi-2D chiral MHPs, Li et al. studied the tuning of molar ratio of chiral-achiral ligands on chiroptical performance. By enhancing the molar ratio of *R/S*-MBABr with respect to achiral component, lower phase formation was favored along with enhancement in CD signal. Importantly, spin lifetime showed an inverse relation with the carrier density, which informs on spin transport and depolarization mechanisms at larger fluence. A green spin-LED was demonstrated with an EQE_{max} of 10.4% and excellent stability as the EL intensity at 535 nm increased constantly with applied bias voltage from 3.5 to 6 V. Furthermore, the g_{EL} was found to be $\approx 5 \times 10^{-2}$, and the majority of CP-EL were attributed to the polarized holes as the lead-bromide based MHPs as known to have p-type character [94].

3.2.3 | Ligand-Engineered Nanocrystals (Chiral Shell / Achiral Core)

Ligand-engineered chiral MHP NCs offer an extrinsic route in which spin selectivity is introduced at the NCs surface by chiral ligands, while EL predominantly originates from the nominally achiral perovskite core. Given the rich surface chemistry of MHPs NCs, ligand engineering plays a pivotal role in optimizing their optoelectronic performance. Controlling ligand density and coverage is crucial for preserving chirality-induced spin filtering while simultaneously minimizing trap states that lead to non-radiative recombination. To this end, ultrasonic-assisted ligand exchange has been reported as an effective strategy for obtaining chiral colloidal MHPs NCs. This technique facilitates better passivation of surface defects, resulting in enhanced PLQY to 94% as compared to 86% (without ultrasonication), reinforcing the structural stability of the MHPs lattice while preserving spin coherence for efficient CPL emission. Using this approach, He et al. demonstrated that chiral MHPs NCs can concurrently act as spin filters and light emitters, achieving a higher g_{EL} of 2.85×10^{-1} and EQE of 16.8%, as shown in Figure 6g–l. The ligand-exchange resulted in an enhanced reported P_{spin} to 86–89% as compared to pristine (P_{spin} of 27–36%) [34].

3.3 | Analysis of Performance Data for Current Spin-LEDs

Data gathered from the studies discussed above are collected in Table 2 and key performance correlations are graphically depicted in Figures 7a,b. The compiled dissymmetry factors reveal a clear gap between chiroptical performance from materials versus devices. Devices exhibiting high g_{EL} often show modest EQE, and vice versa, which has remained an established challenge in spin-LEDs for a range of materials [13]. For example, early spin-LEDs based on chiral methylbenzylammonium in 2D/3D heterostructures reached an EQE of 10.5% with $g_{EL} \approx 5 \times 10^{-2}$, whereas more recent NC-based devices employing lightly chiral-doped MHPs emitters achieved an EQE ≈ 15.4% but with g_{EL} on the order of 10^{-3} [21]. It would seem that structures that minimize transport losses to maximize EQE can dilute spin polarization, whereas strongly chiral architectures enhance g_{EL} at the cost of carrier mobility and additional interfaces. However, this trend is not uniform across all materials. For intrinsically chiral quasi-2D emitters such as *R/S*-$NEA_2(FA_{0.85}Cs_{0.15})_2Pb_3Br_{10}$, g_{EL} (7.8×10^{-2}) closely follows g_{PL} (8.6×10^{-2}), and the near-unity PLQY (~91%) enables an EQE of 13.5% [74]. This deviation is expected when spin selectivity and light emission are co-localized within the same quasi-2D emissive framework, minimizing interfacial spin depolarization during carrier transport. In such intrinsically chiral emitters, g_{EL} therefore approaches g_{PL} indicating that CP-EL is governed primarily by chiral radiative transitions rather than spin-pumping across a separate transport layer. Ultimately, advancing high-performance spin-LEDs requires device designs that concurrently optimize charge transport, spin coherence, and interfacial coupling to deliver both strong CPL and high efficiency.

Spin-LEDs that rely on CISS-driven spin injection from low-dimensional chiral layers tend to show reduced CP-EL under ambient conditions because spin information is partially lost during transport and at interfaces. Ideally, chiral ligands act as spin filters and, at the same time, passivate interfacial defects, aligning carrier spins before recombination so that g_{EL} can substantially exceed the g_{PL}. The embedding chiral organic components throughout the bulk (fully 2D chiral MHPs) generally increases g_{PL} and g_{EL}, potentially due to enhanced lattice distortion and exciton confinement; however, this usually lowers EQE because of the insulating nature of the bulky spacers. A thin 2D chiral MHPs placed beneath a $CsPbI_3$ QD emitter can circumvent the insulation problem, yet the limited QD thickness required to match the short spin-coherence time at room temperature restricts both luminescence and spin selectivity.

In contrast, architectures that use mostly achiral MHPs with only a small amount of chirality (surface ligands or low-fraction chiral dopants) tend to preserve high EQE but yield very small g values. It is therefore desirable to engineer structures in which chiral sub-domains efficiently transfer their spin polarization to high-efficiency emissive domains. Core–shell MHPs QDs with an achiral core and a chiral shell are one such example. To date, 2D or quasi-2D chiral MHPs have been mainly used as shells; however, quasi-2D MHPs such as PEA-based CISS layers exhibit weak spin selectivity and g_{EL} (10^{-3}) because penetration of the chiral cations into the core partially depolarizes the emission [20]. These points toward designing bulkier organic cations that suppress penetration. NEA-based chiral cations, for instance, yield much stronger spin polarization, $g_{EL} \approx 10^{-1}$ and higher PLQY than PEA [89], consistent with a larger magnetic-dipole transition moment and more effective defect passivation [96]. Exploring larger aromatic chiral cations could further enhance

TABLE 2 | Device structures, emission mechanism, and key performance matrices for different spin-LEDs reported in the literature.

Material	Emission Mechanism	CP-EL (nm)	EQE (%)	L_{max} (cd/m^2)	g_{EL}	g_{PL}	PLQY (%)	Turn-on voltage(V)	Operational Lifetime (s)[a]	Ref
(R/S-MBA)$_2$PbI$_4$/CsPbI$_3$ NCs	Extrinsic	688	10.53	≈400	—	—	—	2.4	—	[33]
MAPbBr$_3$/*(R/S-PEA)*	Extrinsic	≈520	3.60	≈1200	6×10^{-3}	4×10^{-3}	54	3.0	—	[20]
CsPbBr$_3$/*(R/S-NEA)*	Extrinsic	505	5.47	1962	2.4×10^{-1}	—	78	2.2	495	[89]
(PEA$_x$)*(R/S-NEAS$_{1-x}$)*2MA$_{n-1}$PbnI$_{3n+1}$	Intrinsic	683	3.70	370	4×10^{-3}	2.1×10^{-3}	31.5	3.4	109	[72]
(2PEA)$_x$*(R/S-2BA)*$_2$MA$_1$CsPb$_3$Br$_{10+x}$	Intrinsic	515	5.21	21240	5.5×10^{-2}	1.96×10^{-3}	60	2.9	—	[75]
MAPbBr3/*(R/S-BinapO)*	Intrinsic	523	3.60	18783	1.8×10^{-1}	5.6×10^{-3}	37.9	3.2	—	[73]
R/S-NEA$_2$(FA$_{0.85}$Cs$_{0.5}$)$_2$Pb$_3$Br$_{10}$	Intrinsic	530	13.5	1084	7.8×10^{-2}	8.6×10^{-2}	91	2.8	1200	[74]
*(2D)(PEA)$_x$(S/R-PRDA)$_{2-X}$*PbBr$_4$/CsPbBr$_3$ NCs	Extrinsic	518	5.70	2280	1.1×10^{-3}	—	—	2.2	—	[58]
(R/S-MBA$_2$PbI$_4$)/(CdSe/ZnS)	Extrinsic	629	2.70	5638	1.6×10^{-2}	—	—	1.9	—	[95]
R/S-bPEABr/CsPbBr$_3$	Intrinsic	519	15.4	12800	2.16×10^{-3}	9.8×10^{-5}	89	2.5	1200	[21]
(2PEA)$_{0.8}$*(R/S-MBA)*$_2$MA$_1$Cs$_1$Pb$_3$Br$_{10.8}$	Extrinsic	518	3.80	9300	5×10^{-2}	1.6×10^{-3}	56	4.0	—	[91]
(t-BA)$_2$*(R/S-MBA)*$_2$MA$_{0.2}$Cs$_{0.8}$Pb$_2$Br$_9$	Extrinsic	520	3.60	4800	1.03×10^{-1}	3.2×10^{-4}	53	4.3	—	[90]
L/D-TBe$_x$(PEA$_{0.6}$iPA$_{0.4}$)$_{2-x}$Cs$_2$Pb$_3$Br$_{10-x}$(BF$_4$)$_x$	Extrinsic	491	12.9	1618	15.8×10^{-2}	8.2×10^{-2}	82.1	3.0	500 (Target) 230 (Control)	[77]
(R/S-MBA)$_2$FA$_2$Pb$_3$Br$_{10}$	Extrinsic	538	15.4	4800	—	—	—	3.2	2150 (R-) 2300 (S-)	[92]
R/S-NEA$_2$(FA$_{0.8}$MA$_{0.2}$)$_2$Pb$_3$Br$_{0.5}$I$_{9.5}$	Extrinsic	782	12.4	—	1.32×10^{-2}	2.6×10^{-2}	86.7	—	735 s	[93]
R/S-MBA/CsPbCl$_{1.5}$Br$_{1.5}$	Extrinsic	520	16.8	28630	2.8×10^{-1}	—	94	2.1	71280	[34]
R/S-MBA/P/M-CsPbX$_3$ NWs	Intrinsic	430	—	—	5×10^{-3}	5.2×10^{-2}	—	—	—	[79]
(R/S-p-F-MBA)$_2$Cs$_1$FA$_1$Pb$_3$I$_{10}$	Intrinsic	728	8.30	—	1.63×10^{-1}	9.4×10^{-2}	—	2.4	—	[76]

[a]T_{50} denotes the time required for the EL intensity to decrease to 50% of its initial value under continuous electrical operation (constant current or constant luminance, as reported).

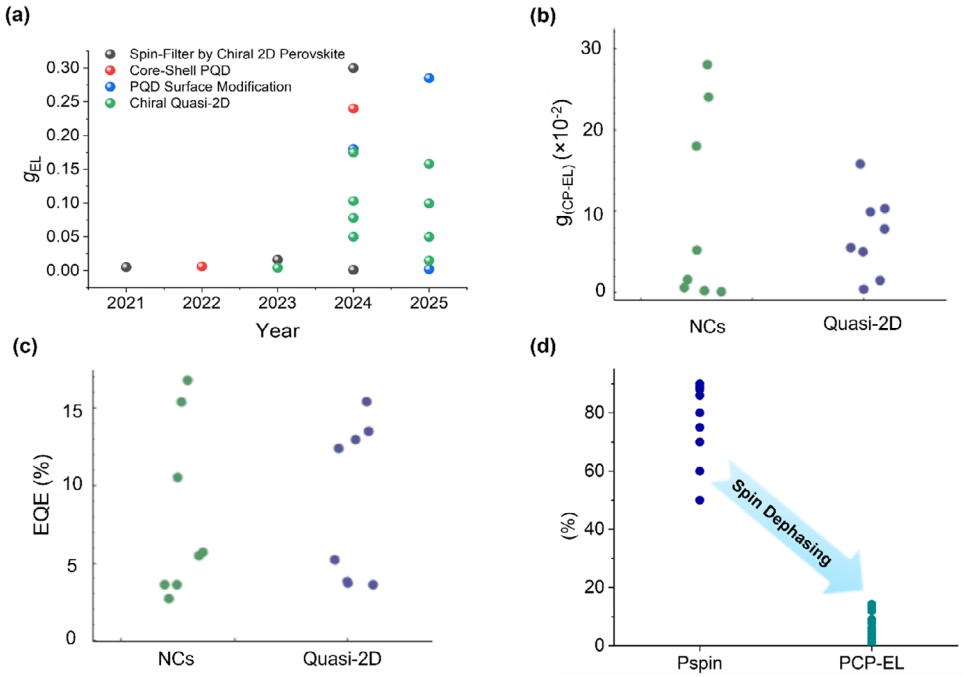

FIGURE 7 | a) A summary of g_{EL} for different materials, b) $g_{(CP-EL)}$, c) EQE (%) of spin-LED devices based on MHPs NCs and quasi-2D chiral MHPs, and d) Impact of spin dephasing on CP-EL.

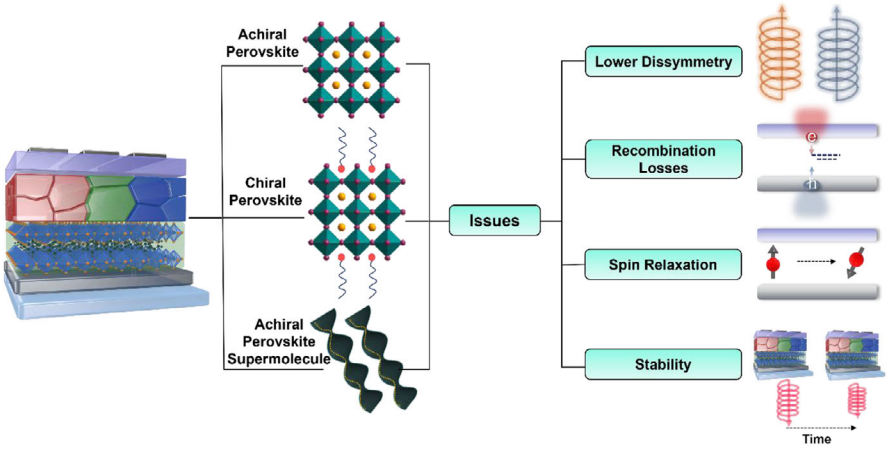

FIGURE 8 | Current limiting factors for chiral MHPs-based spin-LED include lower dissymmetry, recombination losses, spin dynamics, and materials stability.

dissymmetry via stronger chiral electronic coupling, but may also introduce additional lattice strain and hinder charge transport, which motivates the use of chiral MHPs NCs as an alternative platform with improved mobility and film quality.

4 | Overcoming Material and Device Challenges in Spin-LEDs

Even though significant strides have been made for both intrinsic and extrinsic device designs, creating robust, high-performance spin-LEDs still presents a number of interconnected challenges related to materials, interfaces, and device engineering. As highlighted in Figure 8, some of the main hurdles include limited dissymmetry, losses from non-radiative recombination, spin dephasing, and issues with environmental stability. The shift from achiral to chiral MHPs brings exciting new spin-selective functionalities, but it also adds layers of structural and interfacial complexity that can disrupt charge-spin coherence. This is clearly illustrated by the noticeable gap between the reported spin polarization and CP-EL values (Figure 7d). In this section, we discuss the key structural and optical limitations, along with potential strategies to overcome them for realizing efficient spin-LEDs.

4.1 | Dissymmetry Factor

Many of the current studies report small dissymmetry values (10^{-2} to 10^{-3}). It is important to note that such values must be

measured with care, since there are many potential artefacts, such as birefringence, fluorescence anisotropy and optical outcoupling [97]. As we have seen a large variation in g-factors reported, adoption of standardized CPL and CP-EL characterization protocols becomes essential to reliably distinguish intrinsic chiroptical responses from experimental artefacts across different material systems and device architectures. Furthermore, to realize the potential of spin-LEDs in technological applications, the g_{PL} and g_{EL} values should be as high as possible and ideally $>10^{-1}$. For materials used as intrinsic chiral emitters, the product of PLQY and g_{PL} may be used as a key parameter to conveniently evaluate performance [98].

Recent work indicates that achieving this regime does not simply depend on enhancing molecular chirality, but rather on amplifying chirality transfer and intrinsic spin splitting within the inorganic perovskite. For instance, nano-confined growth strategies have been shown to impose controlled micro-strain that strengthens asymmetric H-bonding between chiral spacers and the inorganic framework, leading to pronounced increase in absorption dissymmetry (g_{CD}) and g_{PL} at room temperature [99]. On the other hand, magneto-optical studies have established a direct correlation between the intrinsic exciton spin splitting energy (ΔE_Z) and the *g*-factor, showing that strong chiroptical activity is primarily dictated by the magnitude of spin splitting, rather than by molecular dipole contributions alone. In this context, structural features such as in-plane octahedral tilting and out-of-plane halide displacement play a central role in determining ΔE_Z, and thus set the upper limit for the achievable g-factor [63].

Apart from engineering the chiral molecules directly, integration of MHPs with chiral liquid crystals (CLC) can act as a promising route to enhance the g_{PL}. CLCs provide a long-range ordered self-organized chiral superstructure and can guide the assembly of nanosized luminescent building blocks into highly ordered chiral nanomaterials over larger scales [100, 101]. Several other reports based on different emitter systems, such as chiral fluorescent dyes mixed with liquid crystals, have resulted in enhanced g_{PL} [102]. So, integrating MHPs with the CLC system might be an interesting approach toward formulating a spin-LED. However, it should be noted that the use of CLCs can significantly reduce the luminescence efficiency due to the selective reflection of light by CLCs. While there are several potential methods to combine MHPs with CLCs, one option is chemically cross-link the materials. For instance, Zhang et al. designed liquid crystal-templated chiral system by integrating photo-polymerizable $CsPbX_3$ PQDs into a structurally colored elastic polymer network through cross-linking. This structural integration exhibited excellent chiroptical properties and CPL with a maximum g_{PL} of 1.5 under UV light [103]. On the other hand, Liu et al. demonstrated MHPs and CLC layer-based soft helix resulting in bilayer architecture, where the introduction of polyacrylonitrile (PAN) in the bilayer improved the luminescent efficiency and stability of MHPs while conserving CLC characteristics. Overall, the bilayer resulted in full-color CPL with a high g_{PL} of 1.9 and stability over 6 months at room temperature [104]. Recently, Xu et al. also reported a high g_{PL} of 1.73 based on polymethyl methacrylate (PMMA) or PAN-based $CsPbX_3$ matrix separately stacked with CLC, where the stacking method impacted the handedness of the CPL [105]. To date, however, these LC-templated and polymer-embedded chiral MHPs have not yet been tested at the device level. Exploring how their exceptional chiroptical responses translate under electrical excitation remains an open and promising direction, and will be essential for assessing their potential as active layers in spin-LEDs.

4.2 | Spin Dynamics in Spin-LEDs

Spin dynamics play a critical role in spin-LED performance. In practice, CP-EL is retained only when spin information survives over the timescale relevant to radiative emission, so the key requirement is not merely a long spin lifetime but a favorable timescale matching between spin coherence and recombination. Specifically, radiative recombination should proceed on a timescale comparable to or faster than spin relaxation ($\tau_r \leq \tau_s$); otherwise, rapid spin randomization suppresses spin polarization and reduces CP-EL. This constraint is particularly stringent at non-cryogenic temperatures, where many inorganic semiconductors exhibit short τ_s. [106, 107] In MHPs, τ_s and τ_r are additionally sensitive to defect density, crystallinity, operating temperature, and spin–phonon coupling [108, 109]. Table 3 compiles representative τ_s and τ_r values reported for perovskite systems used in spin-LEDs and shows that τ_r (often obtained from PL/TRPL decays) is frequently much longer than τ_s (typically extracted from time-resolved spin/polarization measurements). This apparent disparity does not necessarily contradict the observation of CP-EL, because PL/TRPL lifetimes commonly represent ensemble-averaged decays that include slow components such as trapping, delayed emission, and other nonradiative pathways, whereas CP-EL can be set by early-time emissive channels or by specific states/domains in which spin information is preferentially retained [109, 110]. In this perspective, we try to address an apparent inconsistency on how chiral NC-based devices can exhibit CP-EL despite picosecond-scale τ_s, while quasi-2D emitters achieve comparatively large dissymmetry without requiring exceptionally long τ_s. The key lies in the balance between spin relaxation and radiative recombination. For instance, in quasi-2D emitter, where energy/spin funneling and the relevant emissive pathways can be ultrafast, may reach comparatively large dissymmetry without requiring long τ_s [93]. However, direct comparison highlights a key methodological limitation, as τ_s and τ_r are often measured under different excitation conditions, probe different carrier/exciton populations, and are reported with non-uniform definitions. Moving forward, more directly comparable datasets, such as co-measuring spin polarization dynamics and emissive recombination under matched excitation/operando conditions with consistent fitting metrics, will be important for establishing clearer design rules for CP-EL retention.

In colloidal MHP NCs, chirality is often introduced extrinsically through chiral surface ligands rather than the inorganic NC core itself, as seen in previous sections [48]. Because spin relaxation in these systems can be dominated by surface scattering and exciton-phonon coupling (e.g., via the Elliott–Yafet (EY) mechanism) [111, 112], chiral ligands may indirectly prolong spin coherence/lifetime by breaking local symmetry, passivating surface traps, and mitigating phonon-assisted scattering, thereby preserving spin polarization up to radiative recombination and strengthening CPL/CP-EL [11].

TABLE 3 | Representative spin lifetime/coherence (τ_s) and recombination timescales (τ_r) in perovskite systems used for spin-LEDs, spanning including intrinsically chiral quasi-2D and 3D emitters, and extrinsic achiral 3D NCs emitters.

Dimensionality	Mechanism	Emission (nm)	τ_s (ps)	τ_r (ns)	Refs.
Quasi-2D	Intrinsic	675	22.0	207.5	[93]
Quasi-2D	Intrinsic	728	87.8	54.8	[93]
Quasi-2D	Intrinsic	782	119.6	55.8	[93]
Quasi-2D (mixed phase)	Intrinsic (internal-heterostructure)	726	27.59	15.44	[76]
Quasi-2D	Intrinsic	491	10.4	16.5	[77]
Quasi-2D (mixed phase)	Intrinsic	528–530	—	1.726	[74]
3D (control)	Intrinsic	528–530	3.0	157.7	[74]
3D NCs	Extrinsic	678	14.2	1.34	[33]
3D NCs	Extrinsic	780	3.86	1.08	[33]
3D NCs	Intrinsic	520	5.9	—	[21]

As seen, 3D MHPs have shown much lower spin lifetime in picosecond range at room temperature as compared to nanosecond range at cryogenic temperature [113, 114]. As a result, strategies such as π-conjugated chiral ligands, stronger binding to NCs surfaces, and rational organic cation engineering can help reduce non-radiative decay and improve spin-polarized charge dynamics [115]. Apart from chiral molecule design, the thickness of the 2D MHPs system plays a vital role in spin relaxation process [116, 117]. It is notable that most of the spin-LEDs reported to date state a CISS-based $P_{spin} \geq 80\%$ whereas, the highest $P_{CP\text{-}EL}$ is $\approx$ 15% ($g_{EL} = 3 \times 10^{-1}$) (Figure 7d), which suggests significant spin dephasing issues. While the details underpinning this disconnect are still being determined, relevant mechanisms to consider include a) EY, b) D'yakonov-Perel (DP), and c) Bir-Aronov-Pikus (BAP) [118].

To expand the range of possible chiral MHPs using materials that are commercially available, a promising avenue is to explore achiral-chiral cation combinations, given the higher availability of achiral components. As described above [42, 43], the interplay between chiral and achiral cations, such as non-covalent aryl-perfluoroaryl interaction and C-H π interaction, impacts the chiroptical activity and spin dynamics. [42, 119, 120] For instance, Sun et al. [56] explored the incorporation of achiral guanidinium (GA^+) and chiral *R*/*S*-methylbenzylammonium in the MHPs inorganic framework. The inclusion of GA^+ led to the formation of an H-bonded network, which induced a highly ordered zigzag chain arrangement with layered stacking. Overall, there was a significant enhancement in the spin-related properties, such as longer spin lifetime ($\approx$7 ns) and higher CISS effect with maximum spin polarization degrees of 92% and -94%. On the other hand, as chiral organic cations have been proven to reduce the PLQY of layered 2D MHPs up to a certain extent due to strong losses from non-radiative recombination, engineering the organic cation structure have shown enhanced PLQY values and chiroptical characteristics in chiral 2D MHPs [30]. Liu et al. [121] tuned the position of halide (Br) atom from para- to meta-position in the (*R*/*S*)-3BrMBA$_2$PbI$_4$ aromatic ring resulted in enhanced PLQY (39%) and CPL of 52%, resulting in g_{PL} of 1 due to higher degree of distortion at room temperature. Interestingly, relaxation dynamics studies via TA spectroscopy revealed that TA decay in the ground state bleach (GSB) of R-3BrMBA$_2$PbI$_4$ is faster than that of R-4BrMBA$_2$PbI$_4$ which might be attributed to suppressed population of nonradiative decay routes in R-3BrMBA$_2$PbI$_4$. Along with reduced non-radiative population, the spin polarization lifetime was found to be in the microsecond(μs) range, which is much longer than usually found in chiral MHPs (ps to ns). This shows the effectiveness of cation engineering on reducing the population of dark states, resulting in faster radiative emission, maintaining circular polarization.

4.3 | Stability of Chiral MHPs Materials

MHPs stability is another crucial factor in determining the long-term performance, operational lifetime, and practical applicability of chiral MHPs LEDs. Due to their potential use in spin-photon interfaces, quantum information technologies, and for high-efficiency CP emission, ensuring the structural and optoelectronic stability of these materials is essential. Among the factors governing stability, the intrinsic structural integrity of the chiral MHPs lattice plays a defining role. In case of chiral NCs, the weak ligand-NC interactions often lead to the detachment of ligands, resulting in a reduction or complete loss of CPL. However, chiral-spin LEDs often show enhanced stability, as compared to traditional MHPs-based LEDs due to the structural modification. For example, organic cations in 2D MHPs, which are effective materials in spin LEDs, serve as hydrophobic barriers and can cap the grain boundaries by forming a 3D network that inhibits ion migration and defect growth [122]. Similarly, the layered (*R*-MBA)$_2$PbBr$_4$ structure is less prone to halide migration at operating biases because the 2D layers block ion movement, leading to more stable EL. Despite these observations, designing chiral MHPs systems with higher stability as well as optoelectronic performance is needed. Some recent

approaches include the introduction of the block copolymer micellar nanoreactor strategy to achieve simultaneous chirality transfer and enhanced stability in MHPs NCs. Unlike traditional ligand-based methods, which suffer from ligand detachment and environmental degradation, the polystyrene-block-poly (2-vinyl pyridine) (PS-B-P2VP) polymer micelle framework forms a supramolecular chiral environment, ensuring robust CPL retention and long-term structural stability [38]. Another study improved the stability of chiral MHPs by leveraging structural isomer-derived H-bonding interactions. By employing naphthyl ethylamine (NEA) cations with different functional group positions (1-NEA *vs*. 2-NEA), the authors demonstrated that 2-NEA-based chiral MHPs exhibits stronger asymmetric H-bonding, leading to greater lattice distortion, enhanced spin polarization, and superior environmental stability under harsh conditions such as 75°C and 75% relative humidity or 1 week. More attention is needed in the engineering of chiral molecules to minimize the interfacial energy losses in LED devices by passivating defects and aligning interfacial energy band simultaneously [123]. Furthermore, to enhance the stability against moisture and humidity, the introduction of hydrophobic groups like isobutyl and benzene-ring-based chiral molecules may be useful. [124]

4.4 | Optical and Scalability Challenges for spin-LED Display Application

As display technologies transition towards micro-/nano-LEDs architectures [125–129], chiral MHPs are emerging as potential materials due to their ability to generate CPL directly at the source level. Their capacity to emit circularly polarized light directly from the emissive layer offers an attractive possibility for simplifying optical stacks and improving efficiency. Viewing angle uniformity is a crucial for spin-LEDs, as it directly affects brightness, contrast ratio, the effective g-factor of polarized light emission under practical operating conditions, and strongly depends on structural and optical factors [130–133]. However, the field is still in its early stages, and several fundamental challenges related to optical design, scalable fabrication, environmental stability must be resolved before practical display integration becomes realistic [134, 135].

Recently, a study demonstrated the development of large-scale one-step, scalable synthesis of producing up to 500 mL of *R*/*S*-$CsPbBr_3$ NCs ink. When incorporated with polymeric matrices such as ethyl cellulose (EC) which acted as both a passivation agent and structural scaffold, these inks exhibited enhanced PLQY and improved environmental stability (≈80% PL intensity after 100 days in air and ≈60% after 30 days in water) and mechanical integrity. Finally, they demonstrated large-area CPL film over centimeter scale using coating techniques, exhibiting consistent g_{lum} across multiple spatial locations [136].

5 | Summary and Outlook

MHPs have recently emerged as a class of materials where chiroptics, optoelectronics, and spintronics meet, providing a versatile way of producing circularly polarized light through intrinsic chirality or the CISS effect. With further developments, the resultant devices are good candidates for future display, quantum photonics, and secure communications. While chiral organic electronics have achieved strong chiroptical properties through molecular and photonic designs, their device performance is often constrained by trade-offs between chirality and charge transport, as well as challenges in controlling molecular orientation and helical stacking. Moreover, under operating conditions (e.g., doping and electric fields), the formation of polaronic/bipolaronic charge states can modify spin-magnetic polarization and charge-transfer pathways, making spin-selective behavior difficult to control reproducibly [137]. In contrast, chiral perovskite spin-LEDs integrate chirality within the hybrid perovskite lattice (via chiral organic cations), such that spin selectivity can be governed largely by band-structure and interfacial spin-filtering effects (e.g., Rashba-type spin splitting and CISS), rather than by the specific molecular packing motifs required in organic semiconductors, often providing improved morphological robustness and comparatively defect-tolerant optoelectronic behavior. As described in this perspective, spin-LEDs based on chiral MHPs can be prepared by two complementary pathways: a) intrinsic chiral emitters, in which the MHPs chiral structure gives rise to CPL, and b) extrinsic spin-pumping, where spin-polarized carriers are generated by the chiral layer, via CISS, and injected into an achiral emissive layer. These two strategies offer a powerful foundation for designing suitable spin LED materials; however, they also highlight the delicate interplay between circular polarization, spin coherence, and structural stability. They also demonstrate other challenges related to broader optoelectronic performance, such as lattice distortion, creating trap states that increase non-radiative recombination and degrade efficiency and stability.

To further increase the g factor beyond the typical (10^{-2}–10^{-3}) range, chiral metasurface-assisted approaches present a promising route [138]. By engineering the resonant photonic modes with strong CD, metasurfaces can amplify light-matter interactions asymmetrically for σ^+ and σ^- photons, effectively enhancing the emission without modulating the intrinsic material chirality. Moreover, the concentration of the chiral ligands and their spatial distribution needs further optimization, as reduced concentration of chiral ligands tends to decrease the optical dissymmetry factor [139]. Beyond surface chemistry, ion doping such as Mn^{2+}, or Co^{2+} has emerged as another effective route to elevated chiral activity and dissymmetry factor [140, 141]. Overall photonic structuring, optical resonance such as plasmonic effects and Mie resonances, metasurfaces with bound states in the continuum (BICs), optical field manipulation, ligand optimization, and dopant engineering offers a promising pathway to achieve higher dissymmetry.

Low-dimensional chiral MHPs NCs and NPLs stand out as promising classes of materials for overcoming such key limitations. Quantum and dielectric confinement within these NCs increase the exciton binding energy and accelerates radiative recombination, reducing spin relaxation and enabling stable EL dissymmetry at room temperature. Within extrinsic spin-filtering architectures, building on the anisotropic NPL systems introduced in Section 3.1.2, anisotropic MHPs NPL films (e.g., $APbX_3$ NPLs) interfaced in a parallel, planar geometry with 2D chiral MHPs offer a distinct and still largely unexplored design space for spin–photon devices. By adjusting NPL thickness, band

alignment, and in-plane orientation, such heterostructures could, in principle, enable polarization-programmable Spin-LEDs with simultaneous control over brightness and the balance between linear and circular polarization–capabilities that are difficult to realize with isotropic NCs or conventional quasi-2D systems.

Furthermore, the use of chiral ligands needs to be carefully studied to further improve chiral properties while simultaneously passivating surface defects. For instance, π-conjugated chiral ligands have shown some promising results in this direction [142], which upon further optimization may help mitigate the usual trade-off between spin polarization and efficiency. Higher g_{PL} may be attained through both intrinsic and extrinsic routes. Intrinsic chirality can be introduced by incorporating chiral organic cations into the MHP framework, whereas extrinsically induced chirality can be achieved by layering chiral ligands onto the surface of NCs, and through superstructure growth of chiral MHPs [30, 143, 144].

Beyond the optimization of chiral MHP materials for spin-LEDs, there is still significant scope for further device design and optimization. For example, it may be possible to integrate the emissive layer with optical cavities, although reflection within the design would need to be carefully considered [145]. For downstream applications, it will be important to address the narrow spectral range that currently limit MHP spin-LEDs [116–118]. Although conventional MHP LEDs have already achieved full-color emission spanning from the NIR to blue, chiral MHPs spin-LEDs still face difficulties in achieving the same spectral coverage [146]. Controlling the bandgap, spin coherence, and chiroptical response all at once across various halide compositions is the main challenge. Cl-based systems that emit blue light have short spin lifetimes and weak spin–orbit coupling, whereas red I-rich MHPs are unstable due to defect formation and halide migration. In order resolve these limitations, broadly applicable chiral ligand frameworks that create strong lattice asymmetry without impeding carrier transport must be combined with compositional and dimensional engineering. New approaches might include multi-emissive heterostructures that take advantage of energy and spin funneling across layered domains, and tandem chiral spin-LED architectures, which stack individual red, green, and blue sub-cells to produce tunable color, broadband CPL emission. Exploring lead-free double MHPs, quantum-well superlattices, and data-driven chirality design may further advance stable, efficient, and color-consistent spin-LED technologies.

Lead-free MHPs also represent an important direction for translating spin-LED concepts toward more technically relevant platforms, yet their promise must be considered in terms of both spin physics and operational stability. Replacing Pb can modify SOC and band-edge symmetry, which in turn may reshape Rashba-type spin splitting and the efficiency of CISS-enabled spin filtering. A critical long-term research direction is the development of lead-free chiral MHP-inspired materials that preserve sufficiently strong SOC, direct-allowed optical transition while maintaining high radiative efficiency. At the same time, stability requirements are likely to become more stringent under electrical bias where the compositions must resist oxidation, defect formation, and ion/vacancy migration, and any chiral functionality must remain robust against ligand desorption. Among potential materials, Sn-based perovskites can provide comparable band structures but remain limited by Sn^{2+} oxidation and instability, while double perovskites and related Bi/Sb-based halides [147] offer improved chemical robustness yet typically suffer from indirect bandgaps and lower radiative efficiency. At present, no lead-free chiral perovskite matches the combined SOC strength, photoluminescence efficiency, and operational stability of Pb-based systems. Importantly progress would benefit from reporting spin-relevant figures of merit alongside standard optoelectronic metrics, for example, the spin polarization and spin-coherence lifetime relative to the radiative recombination timescale, together with continuous-operation lifetime to help understand lead-free compositions application as intrinsic chiral emitters, spin-selective interlayers, or as hybrid architectures in which spin selection and emission are co-localized.

Stability remains one of the central challenges for lead-based chiral perovskites, particularly under ambient conditions where moisture can disrupt structural chirality and accelerate material degradation. As a result, advanced encapsulation strategies are necessary to ensure long-term stability. Importantly, the chiral crystalline framework needs further optimization in terms of defect passivation and hydrophobic coating. Compositional engineering focusing on partial substitution of halide or metal cations (Pb/Sn) might be helpful in reducing lattice strain and suppressing phase instability.

Looking ahead towards the micro-spin-LED future, the integration of defect-engineered chiral MHPs single crystals-based color conversion layer with scalable micro-patterning and optimized optical stacks, and polarization-selective optical elements can offer an attractive pathway for high-resolution spin-LED displays with a control over CPL at pixel level without sacrificing spin coherence or emission efficiency.

At last, a critical bottleneck and limiting factor in the progress of chiral MHPs based spin LEDs is the absence of standardized and reproducible methods for measuring CPL and CP-EL, which makes direct comparison of the key metrics, especially g-factors difficult across different experimental conditions. Advancing the field therefore require consistent characterization protocols, transparent reporting of the CPL spectra, and experimental conditions [97].

Acknowledgements

A.G. acknowledges funding from the Oxford Indira Gandhi Graduate Scholarship at Somerville College Oxford. J.K. acknowledges support from the National Research Foundation of Korea (NRF), funded by the Ministry of Education, through the Postdoctoral Overseas Training Program (Project No. RS-2025-02654026). This material was based on work supported by the Air Force Office of Scientific Research under award number FA9550-23-1-0633 (M.J.F). This work has received funding from the Spanish Agencia Estatal de Investigación (AEI/MCIN) through grants: PID2023-147567NB-I00, funded by MICIU/AEI/10.13039/501100011033. L.P. and S.G.G. acknowledge support from Xunta de Galicia (grant no. ED431F2021/05), and EIC PATHFINDER CHALLENGES project 101162112 (RADIANT), funded by the European Union. R.L.Z.H. acknowledges funding from St. John's College Oxford through the Large Grant, as well as the Royal Academy of Engineering through the Senior Research Fellowship scheme (no. RCSRF/2324-18-68). Funding for open access by the Universidade de Vigo/CISUG.

Conflicts of Interest

The authors declare no conflict of interest.

References

1. S. Pimputkar, J. S. Speck, S. P. Denbaars, and S. Nakamura, "Prospects for LED Lighting," *Nature Photonics* 3 (2009): 180–182.

2. Y. Huang, E. L. Hsiang, M. Y. Deng, and S. T. Wu, "Mini-LED, Micro-LED and OLED Displays: Present Status and Future Perspectives," *Light: Science & Applications* 9 (2020): 105, https://doi.org/10.1038/s41377-020-0341-9.

3. H. W. Chen, J. H. Lee, B. Y. Lin, S. Chen, and S. T. Wu, "Liquid Crystal Display and Organic Light-emitting Diode Display: Present Status and Future Perspectives," *Light: Science & Applications* 7 (2018): 17168.

4. R. Singh, K. N. Narayanan Unni, and A. Solanki, Deepak, "Improving the Contrast Ratio of OLED Displays: An Analysis of Various Techniques," *Optical Materials* 34 (2012): 716–723.

5. Y. Yang, R. C. Da Costa, M. J. Fuchter, and A. J. Campbell, "Circularly Polarized Light Detection by a Chiral Organic Semiconductor Transistor," *Nature Photonics* 7 (2013): 634–638.

6. R. Farshchi, M. Ramsteiner, J. Herfort, A. Tahraoui, and H. T. Grahn, "Optical Communication of Spin Information between Light Emitting Diodes," *Applied Physics Letters* 98 (2011): 162508, https://doi.org/10.1063/1.3582917.

7. Y. Okazaki, M. Kimura, K. Hachiya, and T. Sagawa, "Luminescence-based Circular Polarization Convertors: Polarization Conversion of Linearly Polarized Photoluminescence from One-dimensionally Aligned Quantum Rods Using Retardation Films," *Journal of Materials Chemistry C* 11 (2022): 935–942.

8. W. Su and F. Yuan, "Chiral Perovskites for Room-temperature Spin Light-emitting Diodes," *Science Bulletin* 67 (2022): 1535–1538.

9. E. I. Jung, H. J. Lee, J. Kim, et al., "Recent Progress on Chiral Perovskites as Chiroptical Active Layers for next-generation LEDs," *Materials Science and Engineering: R: Reports* 160 (2024): 100817, https://doi.org/10.1016/j.mser.2024.100817.

10. J. R. Brandt, F. Salerno, and M. J. Fuchter, "The Added Value of Small-molecule Chirality in Technological Applications," *Nature Reviews Chemistry* 1 (2017): 0045, http://doi.org/10.1038/s41570-017-0045.

11. Y. Zhang, S. Yu, B. Han, et al., "Circularly Polarized Luminescence in Chiral Materials," *Matter* 5 (2022): 837.

12. J. Liu, Z. P. Song, L. Y. Sun, B. X. Li, Y. Q. Lu, and Q. Li, "Circularly Polarized Luminescence in Chiral Orientationally Ordered Soft Matter Systems," *Responsive Materials* 1 (2023): 20230005, https://doi.org/10.1002/rpm.20230005.

13. F. Furlan, J. M. Moreno-Naranjo, N. Gasparini, S. Feldmann, J. Wade, and M. J. Fuchter, "Chiral Materials and Mechanisms for Circularly Polarized Light-emitting Diodes," *Nature Photonics* 18 (2024): 658–668.

14. R. Babu, J. E. Heger, T. Dutta, et al., "Chiral Molecules in Action: Chemistry of Chiral Perovskite and Perovskite-Inspired Materials," *ACS Energy Letters* 10 (2025): 5703–5721.

15. J. Crassous, M. J. Fuchter, D. E. Freedman, et al., "Materials for Chiral Light Control," *Nature Reviews Materials* 8 (2023): 365–371.

16. Y. Deng, M. Wang, Y. Zhuang, S. Liu, W. Huang, and Q. Zhao, "Circularly Polarized Luminescence from Organic Micro-/Nano-structures," *Light: Science & Applications* 10 (2021): 76, https://doi.org/10.1038/s41377-021-00516-7.

17. X. Yang, Y. Zhang, T. Zhao, Y. Shi, D. Yang, and X. Jin, "Dynamic Modulation of Circularly Polarized Luminescence in Soft Materials: From Functions to Applications," *Surfaces and Interfaces* 73 (2025): 107511, https://doi.org/10.1016/j.surfin.2025.107511.

18. M. K. Jana, R. Song, H. Liu, et al., "Organic-to-inorganic Structural Chirality Transfer in a 2D Hybrid Perovskite and Impact on Rashba-Dresselhaus Spin-orbit Coupling," *Nature Communications* 11 (2020): 4699, https://doi.org/10.1038/s41467-020-18485-7.

19. Y. Dang, X. Liu, B. Cao, and X. Tao, "Chiral Halide Perovskite Crystals for Optoelectronic Applications," *Matter* 4 (2021): 794.

20. C. Ye, J. Jiang, S. Zou, W. Mi, and Y. Xiao, "Core–Shell Three-Dimensional Perovskite Nanocrystals with Chiral-Induced Spin Selectivity for Room-Temperature Spin Light-Emitting Diodes," *Journal of the American Chemical Society* 144 (2022): 9707–9714.

21. D. Chen, B. Tang, A. A. Sergeev, et al., "Green Spin Light-Emitting Diodes Enabled by Perovskite Nanocrystals in Situ Modified with Chiral Ligands," *ACS Energy Letters* 10 (2025): 815–821.

22. H. Lu, J. Wang, C. Xiao, et al., "Spin-dependent Charge Transport through 2D Chiral Hybrid Lead-iodide Perovskites," *Science Advances* 5 (2019): 7.

23. M. P. Hautzinger, X. Pan, S. C. Hayden, et al., "Room-temperature Spin Injection across a Chiral Perovskite/III–V Interface," *Nature* 631 (2024): 307–312.

24. D. G. Billing and A. Lemmerer, "Bis[(S)-β-phenethylammonium] Tribromoplumbate(II)," *Acta Crystallographica, Section E: Structure Reports Online* 59 (2003): m381–m383, https://doi.org/10.1107/S1600536803010985.

25. N. Mercier, A. L. Barres, M. Giffard, I. Rau, F. Kajzar, and B. Sahraoui, "Conglomerate-to-True-Racemate Reversible Solid-State Transition in Crystals of an Organic Disulfide-Based Iodoplumbate," *Angewandte Chemie International Edition* 45 (2006): 2100–2103.

26. J. Ahn, E. Lee, J. Tan, W. Yang, B. Kim, and J. Moon, "A New Class of Chiral Semiconductors: Chiral-organic-molecule-incorporating Organic–inorganic Hybrid Perovskites," *Materials Horizons* 4 (2017): 851.

27. Y. H. Kim, Y. Zhai, E. A. Gaulding, et al., "Strategies to Achieve High Circularly Polarized Luminescence from Colloidal Organic–Inorganic Hybrid Perovskite Nanocrystals," *ACS Nano* 14 (2020): 8816–8825.

28. Y. Shi, P. Duan, S. Huo, Y. Li, and M. Liu, "Endowing Perovskite Nanocrystals with Circularly Polarized Luminescence," *Advanced Materials* 30 (2018): 1705011, https://doi.org/10.1002/adma.201705011.

29. Z. N. Georgieva, B. P. Bloom, S. Ghosh, and D. H. Waldeck, "Imprinting Chirality onto the Electronic States of Colloidal Perovskite Nanoplatelets," *Advanced Materials* 30 (2018): 1800097, https://doi.org/10.1002/adma.201800097.

30. G. Long, C. Jiang, R. Sabatini, et al., "Spin Control in Reduced-dimensional Chiral Perovskites," *Nature Photonics* 12 (2018): 528–533.

31. H.-Y. Ye, Y.-Y. Tang, P.-F. Li, et al., "Metal-free Three-dimensional Perovskite Ferroelectrics," *Science* 361 (2018): 151.

32. J. Ma, C. Fang, C. Chen, et al., "Chiral 2D Perovskites with a High Degree of Circularly Polarized Photoluminescence," *ACS Nano* 13 (2019): 3659.

33. Y.-H. Kim, Y. Zhai, H. Lu, et al., "Chiral-Induced Spin Selectivity Enables a Room-Temperature Spin Light-Emitting Diode," *Science* 371 (2021) 1129–1133.

34. S. He, W. Lin, D. Yu, et al., "Perovskite Spin Light-emitting Diodes with Simultaneously High Electroluminescence Dissymmetry and High External Quantum Efficiency," *Nature Communications* 16 (2025): 2201, https://doi.org/10.1038/s41467-025-57472-8.

35. J. Son, G. Jang, S. Ma, et al., "Boosted Chirality Transfer in 2D Perovskites through Structural Isomer-Driven Halogen–Halogen Interaction," *Advanced Functional Materials* 35 (2025): 35, https://doi.org/10.1002/adfm.202413041.

36. J. Ma, H. Wang, and D. Li, "Recent Progress of Chiral Perovskites: Materials, Synthesis, and Properties," *Advanced Materials* 33 (2021): 2008785, https://doi.org/10.1002/adma.202008785.

37. H. Lu, Z. V. Vardeny, and M. C. Beard, "Control of Light, Spin and Charge with Chiral Metal Halide Semiconductors," *Nature Reviews Chemistry* 6 (2022): 470–485.

38. J. Son, S. Ma, Y. K. Jung, et al., "Unraveling Chirality Transfer Mechanism by Structural Isomer-derived Hydrogen Bonding Interaction in 2D Chiral Perovskite," *Nature Communications* 14 (2023), https://doi.org/10.1038/s41467-023-38927-2.

39. A. Ishii and T. Miyasaka, "Direct Detection of Circular Polarized Light in Helical 1D Perovskite-Based Photodiode," *Science advances* (2020).

40. J. T. Lin, D. G. Chen, L. S. Yang, et al., "Tuning the Circular Dichroism and Circular Polarized Luminescence Intensities of Chiral 2D Hybrid Organic–Inorganic Perovskites through Halogenation of the Organic Ions," *Angewandte Chemie International Edition* 60 (2021): 21434–21440.

41. W. Choi, M. Kwak, J. Park, et al., "Dimensional Control of Chiral Perovskites for High-performance Circularly Polarized Light Detection via Ligand Engineering," *Chemical Engineering Journal* 498 (2024): 155504, https://doi.org/10.1016/j.cej.2024.155504.

42. L. Yan, M. K. Jana, P. C. Sercel, D. B. Mitzi, and W. You, "Alkyl–Aryl Cation Mixing in Chiral 2D Perovskites," *Journal of the American Chemical Society* 143 (2021): 18114–18120.

43. T. Zhu, X. Li, P. Yu, et al., "Rational Design of Enantiomeric Lead-free Double Perovskites by Achiral-chiral Cation Intercalation," *Chemistry* 10 (2024): 882–890.

44. H. Song, M. Kwak, W. Choi, D. Yoo, and J. H. Oh, "Enhancing Circular Dichroism in Chiral Perovskites via Dual Spacer Cation Engineering for Circularly Polarized Light Detection," *Advanced Optical Materials* 12 (2024): 2401427, https://doi.org/10.1002/adom.202401427.

45. G. Chen, X. Liu, J. An, et al., "Nucleation-mediated Growth of Chiral 3D Organic–inorganic Perovskite Single Crystals," *Nature Chemistry* 15 (2023): 1581–1590.

46. A. Forde, D. Ghosh, D. Kilin, A. C. Evans, S. Tretiak, and A. J. Neukirch, "Induced Chirality in Halide Perovskite Clusters through Surface Chemistry," *The Journal of Physical Chemistry Letters* 13 (2022): 686–693.

47. P. C. Sercel, M. P. Hautzinger, R. Song, V. Blum, and M. C. Beard, "Optical Activity of Chiral Excitons," *Advanced Materials* 37 (2025): 2415901, https://doi.org/10.1002/adma.202415901.

48. Y. H. Kim, R. Song, J. Hao, et al., "The Structural Origin of Chiroptical Properties in Perovskite Nanocrystals with Chiral Organic Ligands," *Advanced Functional Materials* 32 (2022): 2200454.

49. J. Mendoza-Carreño, P. Molet, C. Otero-Martínez, M. I. Alonso, L. Polavarapu, and A. Mihi, "Nanoimprinted 2D-Chiral Perovskite Nanocrystal Metasurfaces for Circularly Polarized Photoluminescence," *Advanced Materials* 35 (2023): 2210477.

50. H. Kim, C. A. Figueroa Morales, S. Seong, Z. Hu, and X. Gong, "Perovskite-Supramolecular Co-Assembly for Chiral Optoelectronics," *ACS Applied Materials & Interfaces* 16 (2024): 16515–16521.

51. Y. Lu, Q. Wang, R. He, et al., "Highly Efficient Spin-Filtering Transport in Chiral Hybrid Copper Halides," *Angewandte Chemie International Edition* 60 (2021): 23578–23583.

52. Y. Lu, Q. Wang, R. Chen, et al., "Spin-Dependent Charge Transport in 1D Chiral Hybrid Lead-Bromide Perovskite with High Stability," *Advanced Functional Materials* 31 (2021): 2104605, https://doi.org/10.1002/adfm.202104605.

53. Q. Wang, Y. Lu, R. L. He, et al., "Spin Selectivity in Chiral Hybrid Cobalt Halide Films with Ultrasmooth Surface," *Small Methods* 6 (2022): 2201048.

54. H. Li, R. Cao, M. Tao, J. Jiang, and Y. Xiao, "Chiral Perovskites with a Unique 1D Chain Structure: Impact of Chiral Ligand Geometry on Local Inversion Asymmetry and Chiral-induced Spin Selectivity," *Chemical Science* 16 (2025): 4057–4065.

55. S. H. Nam, J. An, W. Jeong, et al., "Structural Asymmetry and Chiral-Induced Spin Selectivity in Chiral Palladium-Halide Semiconductors," *Journal of the American Chemical Society* 146 (2024): 15045–15052.

56. S. Sun, J. Jiang, M. Jia, Y. Tian, and Y. Xiao, "1.5D Chiral Perovskites Mediated by Hydrogen-Bonding Network with Remarkable Spin-Polarized Property," *Angewandte Chemie International Edition* 64 (2025): 202423314, https://doi.org/10.1002/anie.202423314.

57. A. Maiti and A. J. Pal, "Spin-Selective Charge Transport in Lead-Free Chiral Perovskites: The Key towards High-Anisotropy in Circularly-Polarized Light Detection," *Angewandte Chemie – International Edition* 61 (2022): 202214161, https://doi.org/10.1002/anie.202214161.

58. L. Z. Feng, Y. H. Song, Z. Du Li, et al., "Dimensional and Doping Engineering of Chiral Perovskites with Enhanced Spin Selectivity for Green Emissive Spin Light-Emitting Diodes," *Nano Letters* 24 (2024): 6084–6091.

59. L. S. Yang, C. Y. Huang, C. A. Hsu, et al., "Solution-processed Spin Organic Light-emitting Diodes Based on Antisolvent-treated 2D Chiral Perovskites with Strong Spin-dependent Carrier Transport," *Materials Horizons* 12 (2024): 1863–1877.

60. H. Lu, C. Xiao, R. Song, et al., "Highly Distorted Chiral Two-Dimensional Tin Iodide Perovskites for Spin Polarized Charge Transport," *Journal of the American Chemical Society* 142 (2020): 13030–13040.

61. R. Babu, H. Xu, B. Covelo, et al., "Chiral Molecules Induce Enantiomorphic Lattice Helicity in Chiral 0D Tin Bromide Crystals," *Angewandte Chemie International Edition* 64 (2025): 202510842, https://doi.org/10.1002/anie.202510842.

62. H. Lu, J. Wang, C. Xiao, et al., "Spin-Dependent Charge Transport through 2D Chiral Hybrid Lead-Iodide Perovskites," *Science Advances* 5 (2019): eaay0571.

63. Z. Zhang, J. Wu, and H. Lu, "Deciphering the Electronic and Structural Origin of Chiroptical Activity of Chiral 2D Perovskites," *Chemical Science* 15 (2024): 20440–20447.

64. E. Lafalce, E. Amerling, Z. G. Yu, P. C. Sercel, L. Whittaker-Brooks, and Z. V. Vardeny, "Rashba Splitting in Organic–inorganic Lead–halide Perovskites Revealed through Two-photon Absorption Spectroscopy," *Nature Communications* 13 (2022): 483, https://doi.org/10.1038/s41467-022-28127-9.

65. S. Ma, J. Ahn, and J. Moon, "Chiral Perovskites for Next-Generation Photonics: From Chirality Transfer to Chiroptical Activity," *Advanced Materials* 33 (2021): 2005760, https://doi.org/10.1002/adma.202005760.

66. N. Laxmi, P. Srinivasan, and D. Kabra, "Optical and Optoelectronic Properties of 2D, Quasi-2D and 3D Metal Halide Perovskites," *Journal of Materials Chemistry C* 13 (2025): 13620–13646.

67. S. Ghosh, B. Pradhan, A. Bandyopadhyay, et al., "Rashba-Type Band Splitting Effect in 2D (PEA) 2 PbI 4 Perovskites and Its Impact on Exciton–Phonon Coupling," *The Journal of Physical Chemistry Letters* 15 (2024): 7970–7978.

68. M. K. Jana, R. Song, Y. Xie, et al., "Structural Descriptor for Enhanced Spin-splitting in 2D Hybrid Perovskites," *Nature Communications* 12 (2021): 4982, https://doi.org/10.1038/s41467-021-25149-7.

69. J. Wang, C. Zhang, H. Liu, et al., "Tunable Spin Characteristic Properties in Spin Valve Devices Based on Hybrid Organic–Inorganic Perovskites," *Advanced Materials* 31 (2019): 1904059, https://doi.org/10.1002/adma.201904059.

70. B. Liu, H. Gao, C. Meng, and H. Ye, "The Impact of an External Electric Field on the Rashba Effect in Two-dimensional Hybrid Perovskites," *Journal of Materials Chemistry C* 11 (2023): 10370–10376.

71. B. Wu, H. Yuan, Q. Xu, et al., "Indirect Tail States Formation by Thermal-induced Polar Fluctuations in Halide Perovskites," *Nature Communications* 10 (2019): 484, https://doi.org/10.1038/s41467-019-08326-7.

72. C. H. Yang, S. B. Xiao, H. Xiao, L. J. Xu, and Z. N. Chen, "Efficient Red-Emissive Circularly Polarized Electroluminescence Enabled by Quasi-2D Perovskite with Chiral Spacer Cation," *ACS Nano* 17 (2023): 7830–7836.

73. C. H. Yang, H. Xiao, Y. F. Sang, et al., "In Situ Formed Perovskite Nanocrystal Films toward Efficient Circularly Polarized Electroluminescence," *Advanced Functional Materials* 34 (2024): 2310500, https://doi.org/10.1002/adfm.202310500.

74. J. Yao, Z. Wang, Y. Huang, et al., "Efficient Green Spin Light-Emitting Diodes Enabled by Ultrafast Energy- and Spin-Funneling in Chiral Perovskites," *Journal of the American Chemical Society* 146 (2024): 14157–14165.

75. X. Yan, R. Cao, R. Zhang, H. Gao, and Y. Xiao, "Mixed-Ligand Chiral Quasi-2D Perovskites for Standard and Deep Blue CP-LEDs," *Advanced Functional Materials* 34 (2024): 2410012, https://doi.org/10.1002/adfm.202410012.

76. L. Jiang, G. Zhang, H. Chen, et al., "Self-Assembled Monolayers Facilitate Simultaneous Enhancements of External Quantum Efficiencies and Circularly Polarized Luminescence Dissymmetry Factors for Chiral Perovskite Red Spin-Light Emitting Diodes," *Advanced Science* 13 (2025): 12057, https://doi.org/10.1002/advs.202512057.

77. G. Zhang, J. Tang, Y. Li, et al., "High-Performance Sky-Blue Perovskite Spin-Light Emitting Diodes due to Chiral Ionic Liquid Implantation and Passivation," *Advanced Functional Materials* 35 (2025): 2503088, https://doi.org/10.1002/adfm.202503088.

78. J. Ren, B. Dong, X. Zhou, et al., "Amplifying the Circularly Polarized Luminescence of CsPbBr 3 Nanocrystals by Chiral Metal–Organic Frameworks: In-Situ Growth, Chiral Assemble, and Chirality Transfer," *Advanced Functional Materials* 36 (2025): 22001, https://doi.org/10.1002/adfm.202522001.

79. G. Chen, K. Zhou, Q. Liu, et al., "Chiral All-Inorganic Perovskite Subnanowires," *Journal of the American Chemical Society* 147 (2025): 12347–12359.

80. T. Wang, Z. Li, M. Ge, et al., "Polar Solvent-Assisted Chiral Ligand and Cation Exchange for Bright, Strongly Circularly Polarized Emission in CsPbBr 3 Perovskite Nanoplatelets," *Advanced Optical Materials* 13 (2025): 02519, https://doi.org/10.1002/adom.202502519.

81. B. Zhao, M. Vasilopoulou, A. Fakharuddin, et al., "Light Management for Perovskite Light-emitting Diodes," *Nature Nanotechnology* 18 (2023): 981–992.

82. B. P. Bloom, Y. Paltiel, R. Naaman, and D. H. Waldeck, "Chiral Induced Spin Selectivity," *Chemical Reviews* 124 (2024): 1950–1991.

83. Y. Wang, M. Sen Song, J. Zhao, et al., "Chiral Perovskite Heterostructure Films of CsPbBr 3 Quantum Dots and 2D Chiral Perovskite with Circularly Polarized Luminescence Performance and Energy Transfer," *ACS Nano* 18 (2024): 22334–22343.

84. Z. Nazir, N. Liu, M. A. Khan, et al., "Chirality-Induced Spin Selectivity in II-VI and III-V Semiconductor Nanocrystals: Mechanism, Manipulation, and Application," *Advanced Optical Materials* 14 (2025): 02769, https://doi.org/10.1002/adom.202502769.

85. H. Lee, C. U. Lee, J. Yun, et al., "A Dual Spin-controlled Chiral Two-/Three-dimensional Perovskite Artificial Leaf for Efficient Overall Photoelectrochemical Water Splitting," *Nature Communications* 15 (2024): 4672, https://doi.org/10.1038/s41467-024-49216-x.

86. B. Kwon, J. Park, W. Choi, H. Song, and J. H. Oh, "Ligand-Driven Chirality in Perovskites for Advanced Optoelectronics," *ACS Applied Materials & Interfaces* 17 (2025): 54356–54379.

87. S. Ramakrishnan, Y. Dong, Y. Xie, et al., "Layer Number Dependence of Chirality and Spin Polarized Lifetime in Chiral 2D Halide Perovskites," *Journal of the American Chemical Society* 147 (2025): 44457–44467.

88. J. Xiao, Y. Li, Y. Liu, et al., "Precision Engineering Chiral Interfaces for Efficient Spin Injection in Metal Halide Heterostructures," *Nature Communications* (2026), https://doi.org/10.1038/s41467-026-69455-4.

89. G. Jang, D. Y. Jo, S. Ma, et al., "Core–Shell Perovskite Quantum Dots for Highly Selective Room-Temperature Spin Light-Emitting Diodes," *Advanced Materials* 36 (2024): 2309335, https://doi.org/10.1002/adma.202309335.

90. R. Zhang, Y. Tian, C. Ye, et al., "Efficient Quasi-2D Perovskite Spin Light-Emitting Diodes Based on Chiral-Induced Spin Selectivity," *Chemistry of Materials* 36 (2024): 3812–3819.

91. H. Gao, Y. Chen, R. Zhang, et al., "Dual-ligand Quasi-2D Perovskites with Chiral-induced Spin Selectivity for Room Temperature Spin-LEDs," *Materials Horizons* 11 (2024): 2906.

92. B. Li, Y. Li, W. Yuan, et al., "Chiral Quasi-2D Perovskites Based Single Junction Spin-Light-Emitting Diodes," *Advanced Functional Materials* 35 (2025): 2415433, https://doi.org/10.1002/adfm.202415433.

93. J. Yao, Y. Huang, H. Sun, et al., "Efficient Spin-Light-Emitting Diodes with Tunable Red to Near-Infrared Emission at Room Temperature," *Advanced Materials* 37 (2025): 2413669, https://doi.org/10.1002/adma.202413669.

94. Y. Li, L. Jiang, J. Tang, et al., "Unraveling Chiral Perovskite Spin-Light Emitting Diode Performance and Magneto-Chiroptical Properties Relationship due to the Synergistic Effect," *Advanced Functional Materials* 35 (2025): 2424619, https://doi.org/10.1002/adfm.202424619.

95. Q. Wang, H. Zhu, Y. Tan, et al., "Spin Quantum Dot Light-Emitting Diodes Enabled by 2D Chiral Perovskite with Spin-Dependent Carrier Transport," *Advanced Materials* 36 (2024): 2305604, https://doi.org/10.1002/adma.202305604.

96. J. Ahn, S. Ma, J. Y. Kim, et al., "Chiral 2D Organic Inorganic Hybrid Perovskite with Circular Dichroism Tunable over Wide Wavelength Range," *Journal of the American Chemical Society* 142 (2020): 4206–4212.

97. H. Lu, L. Di Bari, and L. Favereau, "Standardizing the Characterization of Circularly Polarized Luminescence of Chiral Materials," *Nature Photonics* 19 (2025): 1041–1047, https://doi.org/10.1038/s41566-025-01729-7.

98. L. Yao, G. Niu, J. Li, et al., "Circularly Polarized Luminescence from Chiral Tetranuclear Copper(I) Iodide Clusters," *The Journal of Physical Chemistry Letters* 11 (2020): 1255–1260.

99. S. Ma, Y. K. Jung, J. Ahn, et al., "Elucidating the Origin of Chiroptical Activity in Chiral 2D Perovskites through Nano-confined Growth," *Nature Communications* 13 (2022): 3259, https://doi.org/10.1038/s41467-022-31017-9.

100. M. Yuan, X. Wen, X. F. Jiang, L. Polavarapu, G. Zhou, and X. Hu, "Circularly Polarized Luminescent Halide Perovskites: Research Progress and Prospective," *Laser & Photonics Reviews* 19 (2025): 02178, https://doi.org/10.1002/lpor.202402178.

101. W. Lin, C. Yang, Y. Miao, et al., "Toward Chiral Lasing from all-Solution-Processed Flexible Perovskite-Nanocrystal–Liquid-Crystal Membranes," *Advanced Materials* 35 (2023): 2301573, https://doi.org/10.1002/adma.202301573.

102. J. Liu, L. Xu, N. Yang, C. Hu, and Y. Yang, "Enhancing Circularly Polarized Luminescence in Chiral Fluorescent Dyes via Cholesteric Liquid Crystal Polymer Networks," *ACS Applied Polymer Materials* 7 (2025): 4029–4037.

103. X. Zhang, L. Li, Y. Chen, et al., "Mechanically Tunable Circularly Polarized Luminescence of Liquid Crystal-Templated Chiral Perovskite Quantum Dots," *Angewandte Chemie International Edition* 63 (2024): 202404202, https://doi.org/10.1002/anie.202404202.

104. S. Liu, X. Liu, Y. Wu, et al., "Circularly Polarized Perovskite Luminescence with Dissymmetry Factor up to 1.9 by Soft Helix Bilayer Device," *Matter* 5 (2022): 2319.

105. L. Xu, H. Lei, Z. Li, W. Liu, Y. Li, and Y. Yang, "Circularly Polarized Luminescence with Large Dissymmetry Factors Based on Perovskite and Cholesteric Liquid Crystal Polymer Network Films," *Journal of Materials Chemistry C* 13 (2025): 7544–7549.

106. J. Wang, C. Zhang, H. Liu, et al., "Spin-optoelectronic Devices Based on Hybrid Organic-inorganic Trihalide Perovskites," *Nature Communications* 10 (2019): 129, https://doi.org/10.1038/s41467-018-07952-x.

107. M. A. Haque and M. C. Beard, "Spin Effects in Metal Halide Perovskite Semiconductors," *Nanoscale* 17 (2025): 9895–9906.

108. J. Xu, K. Li, U. N. Huynh, et al., "How Spin Relaxes and Dephases in Bulk Halide Perovskites," *Nature Communications* 15 (2024): 188, https://doi.org/10.1038/s41467-023-42835-w.

109. V. V. Belykh, D. R. Yakovlev, M. M. Glazov, et al., "Coherent Spin Dynamics of Electrons and Holes in CsPbBr3 Perovskite Crystals," *Nature Communications* 10 (2019): 673, https://doi.org/10.1038/s41467-019-08625-z.

110. M. A. Becker, C. Bernasconi, M. I. Bodnarchuk, et al., "Unraveling the Origin of the Long Fluorescence Decay Component of Cesium Lead Halide Perovskite Nanocrystals," *ACS Nano* 14 (2020): 14939–14946.

111. R. Cai, I. Wadgaonkar, J. W. M. Lim, et al., "Zero-field Quantum Beats and Spin Decoherence Mechanisms in CsPbBr3 Perovskite Nanocrystals," *Nature Communications* 14 (2023): 2472, https://doi.org/10.1038/s41467-023-37721-4.

112. S. Strohmair, A. Dey, Y. Tong, L. Polavarapu, B. J. Bohn, and J. Feldmann, "Spin Polarization Dynamics of Free Charge Carriers in CsPbI 3 Nanocrystals," *Nano Letters* 20 (2020): 4724–4730.

113. D. Giovanni, H. Ma, J. Chua, et al., "Highly Spin-Polarized Carrier Dynamics and Ultralarge Photoinduced Magnetization in CH 3 NH 3 PbI 3 Perovskite Thin Films," *Nano Letters* 15 (2015): 1553–1558.

114. P. Odenthal, W. Talmadge, N. Gundlach, et al., "Spin-polarized Exciton Quantum Beating in Hybrid Organic–inorganic Perovskites," *Nature Physics* 13 (2017): 894–899.

115. L. Yang, Y. Gao, Y. Zhai, and M. Shao, "Unraveling the Impact of Organic Cation Dipole Moment on Rashba Spin-Splitting in 2D Hybrid Organic–Inorganic Perovskites," *Angewandte Chemie International Edition* 64 (2025): 202507829, https://doi.org/10.1002/anie.202507829.

116. X. Chen, H. Lu, K. Wang, et al., "Tuning Spin-Polarized Lifetime in Two-Dimensional Metal–Halide Perovskite through Exciton Binding Energy," *Journal of the American Chemical Society* 143 (2021): 19438–19445.

117. X. Chen, H. Lu, Z. Li, et al., "Impact of Layer Thickness on the Charge Carrier and Spin Coherence Lifetime in Two-Dimensional Layered Perovskite Single Crystals," *ACS Energy Letters* 3 (2018): 2273–2279.

118. A. Privitera, M. Righetto, F. Cacialli, and M. K. Riede, "Perspectives of Organic and Perovskite-Based Spintronics," *Advanced Optical Materials* 9 (2021): 2100215, https://doi.org/10.1002/adom.202100215.

119. Q. Guan, T. Zhu, Z. K. Zhu, et al., "Unprecedented Chiral Three-Dimensional Hybrid Organic-Inorganic Perovskitoids," *Angewandte Chemie International Edition* 62 (2023): 202307034, https://doi.org/10.1002/anie.202307034.

120. T. Zhu, W. Weng, C. Ji, et al., "Chain-to-Layer Dimensionality Engineering of Chiral Hybrid Perovskites to Realize Passive Highly Circular-Polarization-Sensitive Photodetection," *Journal of the American Chemical Society* 144 (2022): 18062–18068.

121. S. Liu, M. Kepenekian, S. Bodnar, et al., "Bright Circularly Polarized Photoluminescence in Chiral Layered Hybrid Lead-Halide Perovskites," *Science Advances* (2023).

122. M. P. Arciniegas and L. Manna, "Designing Ruddlesden–Popper Layered Perovskites through Their Organic Cations," *ACS Energy Letters* 7 (2022): 2944–2953.

123. J. Son, S. Ma, Y. K. Jung, et al., "Unraveling Chirality Transfer Mechanism by Structural Isomer-derived Hydrogen Bonding Interaction in 2D Chiral Perovskite," *Nature Communications* 14 (2023): 3124, https://doi.org/10.1038/s41467-023-38927-2.

124. P. Kumar, S. K. Sharma, and R. Singh, "A Hydrophobic Organic Spacer Cation for Improving Moisture Resistance and Efficiency in Mixed-dimensional Perovskite Solar Cells," *EES Solar* 1 (2025): 356.

125. A. Gaurav, C. S. Chen, C. Y. Tsai, Z. T. Ye, and C. F. Lin, "Stable Colour Conversion Layer with Enhanced Conversion Efficiency by Incorporating Nanoparticles for Micro-LED Display Application," *Materials Today Chemistry* 39 (2024): 102184, https://doi.org/10.1016/j.mtchem.2024.102184.

126. A. Gaurav, C.-Y. Tsai, G.-W. Wang, H.-Y. Tsai, Z. T. Ye, and C.-F. Lin, "Ultrahigh-resolution Full-color Micro-LED Array with Enhanced Efficiency Based on a Color Conversion Technique," *Photonics Research* 11 (2023): 925.

127. M. Yuan, J. Feng, H. Li, et al., "Remote Epitaxial Crystalline Perovskites for Ultrahigh-resolution Micro-LED Displays," *Nature Nanotechnology* 20 (2025): 381–387, https://doi.org/10.1038/s41565-024-01841-9.

128. X. Wang, Z. Tian, S. Pei, et al., "Highly Efficient Linearly Polarized LED via Surface Plasmon Integrated with Ag Nanocone Metasurface," *Applied Physics Letters* 127 (2025): 073301, https://doi.org/10.1063/5.0282759.

129. X. Gao, Y. Xu, J. Huang, et al., "Circularly Polarized Light Emission from a GaN Micro-LED Integrated with Functional Metasurfaces for 3D Display," *Optics Letters* 46 (2021): 2666.

130. Y. Lee, H. Kim, and C. Kim, "Rigorous Optical Modeling of Circularly Polarized Light-Emitting Devices: Interaction of Emitters with Device Geometries," *ACS Photonics* 10 (2023): 3283–3290.

131. D. Okada and F. Araoka, "Magneto-Chiral Nonlinear Optical Effect with Large Anisotropic Response in Two-Dimensional Halide Perovskite," *Angewandte Chemie International Edition* 63 (2024): 202402081, https://doi.org/10.1002/anie.202402081.

132. F. Zinna, M. Pasini, F. Galeotti, C. Botta, L. Di Bari, and U. Giovanella, "Design of Lanthanide-Based OLEDs with Remarkable Circularly Polarized Electroluminescence," *Advanced Functional Materials* 27 (2017): 1603719, https://doi.org/10.1002/adfm.201603719.

133. F. Zinna, G. Pescitelli, and L. Di Bari, "Circularly Polarized Light at the Mirror: Caveats and Opportunities," *Chirality* 32 (2020): 765–769.

134. D. Gromyko, S. An, S. Gorelik, et al., "Unidirectional Chiral Emission via Twisted Bi-layer Metasurfaces," *Nature Communications* 15 (2024): 9804, https://doi.org/10.1038/s41467-024-54262-6.

135. L. Kang, S. P. Rodrigues, M. Taghinejad, et al., "Preserving Spin States Upon Reflection: Linear and Nonlinear Responses of a Chiral Meta-Mirror," *Nano Letters* 17 (2017): 7102–7109.

136. B. Li, L. Xu, W. Fan, F. Wang, W. Wang, and J. Song, "Scale-up Synthesis of Perovskite Nanocrystal/Cellulose Chiral Ink toward Patterned and Circularly Polarized Luminescence," *Materials Futures* 5 (2026): 025301, https://doi.org/10.1088/2752-5724/ae3592.

137. H. Lee, D. Kim, J. H. Cho, and J. A. Lim, "Facile Strategies for Incorporating Chiroptical Activity into Organic Optoelectronic Devices," *Accounts of Materials Research* 6 (2025): 434–446.

138. N. Fiuza-Maneiro, J. Mendoza-Carreño, S. Gómez-Graña, M. I. Alonso, L. Polavarapu, and A. Mihi, "Inducing Efficient and Multiwavelength Circularly Polarized Emission from Perovskite Nanocrystals Using Chiral Metasurfaces," *Advanced Materials* 36 (2024): 2413967, https://doi.org/10.1002/adma.202413967.

139. Y. Wang, F. Lu, M. Liao, W. Liu, D. Wu, and K. Wang, "Recent Advances in Spin-LEDs Based on Chiral Nanomaterials: Bridging Fundamental Physics, Materials, and Devices Performance," *Advanced Optical Materials* 13 (2025): 02273, https://doi.org/10.1002/adom.202502273.

140. Y. Liu, Y. Jiang, Z. Xu, et al., "Magnetic Doping Induced Strong Circularly Polarized Light Emission and Detection in 2D Layered Halide Perovskite," *Advanced Optical Materials* 10 (2022): 2200183, https://doi.org/10.1002/adom.202200183.

141. Z. Zhang, W. Liang, J. Xue, X. Li, K. Wu, and H. Lu, "Induced Circularly Polarized Luminescence and Exciton Fine Structure Splitting in Magnetic-Doped Chiral Perovskites," *ACS Nano* 18 (2023): 5890–5897, https://doi.org/10.1021/acsnano.3c12851.

142. Y. Yang, L. Liu, and Z. Wei, "Chiral Conjugated Molecular Assemblies Interact with Substances and Light," *Accounts of Materials Research* 5 (2024): 329–346.

143. X. Liu, A. Chanana, U. Huynh, et al., "Circular Photogalvanic Spectroscopy of Rashba Splitting in 2D Hybrid Organic–inorganic Perovskite

Multiple Quantum Wells," *Nature Communications* 11 (2020): 323, https://doi.org/10.1038/s41467-019-14073-6.

144. C. Chen, L. Gao, W. Gao, et al., "Circularly Polarized Light Detection Using Chiral Hybrid Perovskite," *Nature Communications* 10 (2019): 1927, https://doi.org/10.1038/s41467-019-09942-z.

145. T. L. Chen, A. Salij, K. A. Parrish, et al., "A 2D Chiral Microcavity Based on Apparent Circular Dichroism," *Nature Communications* 15 (2024): 3072, https://doi.org/10.1038/s41467-024-47411-4.

146. A. Gaurav, Y. Lu, J. Shamsi, and M. Abdi-Jalebi, "Multi-color Perovskite Light-emitting Diode via Color Conversion and Tandem Architecture," *Matter* 8 (2025): 102417, https://doi.org/10.1016/j.matt.2025.102417.

147. J. Hu, X. Wen, D. Yang, Y. Chen, Z. Liu, and D. Li, "Lead-Free Chiral Perovskite for High Degree of Circularly Polarized Light Emission and Spin Injection," *Nano Letters* 24 (2024): 1001–1008.